Pontifícia Universidade Católica
do Rio de Janeiro

Lucas Ferreira Lima dos Santos

Mechanical performance of an ortho-planar spring compliant mechanism after aging tests

Dissertação de Mestrado

Thesis presented to the Programa de Pós–graduação em Engenharia de Materiais e de Processos Químicos e Metalúrgicos of PUC-Rio in partial fulfillment of the requirements for the degree of Mestre em Engenharia de Materiais e de Processos Químicos e Metalúrgicos.

Advisor: Prof. José Roberto Moraes d'Almeida

Rio de Janeiro
August 2021

Lucas Ferreira Lima dos Santos

Mechanical performance of an ortho-planar spring compliant mechanism after aging tests

Thesis presented to the Programa de Pós–graduação em Engenharia de Materiais e de Processos Químicos e Metalúrgicos of PUC-Rio in partial fulfillment of the requirements for the degree of Mestre em Engenharia de Materiais e de Processos Químicos e Metalúrgicos. Approved by the undersigned Examination Committee.

Prof. José Roberto Moraes d'Almeida
Advisor
Departamento de Engenharia Química e de Materiais – PUC-Rio

Prof. Daniel Carlos Taissum Cardoso
Departamento de Engenharia Civil e Meio Ambiente – PUC-Rio

Prof. Flávio de Andrade Silva
Departamento de Engenharia Civil e Meio Ambiente – PUC-Rio

Rio de Janeiro, August the 28th, 2021

Lucas Ferreira Lima dos Santos

He got a degree in Mechanical Engineering from Rio de Janeiro State University (UERJ) in 2019. During the Master's degree, he worked in a project funded by Petrobras aimed at studying composite repairs in oil pipes.

Bibliographic data

Santos, Lucas Ferreira Lima dos

Mechanical performance of an ortho-planar spring compliant mechanism after aging tests / Lucas Ferreira Lima dos Santos; advisor: José Roberto Moraes d'Almeida. – Rio de janeiro: PUC-Rio, Departamento de Engenharia Química e de Materiais, 2021.

v., 101 f: il. color. ; 30 cm

Dissertação (mestrado) - Pontifícia Universidade Católica do Rio de Janeiro, Departamento de Engenharia Química e de Materiais.

Inclui bibliografia

1. Engenharia Química – Teses. 2. Engenharia de Materiais – Teses. 3. Mecanismos flexíveis;. 4. Envelhecimento higrotermal;. 5. Envelhecimento com UV;. 6. Mola orto-planar;. 7. Manufatura aditiva.. I. d'Almeida, José Roberto Moraes. II. Pontifícia Universidade Católica do Rio de Janeiro. Departamento de Engenharia Química e de Materiais. III. Título.

CDD: 620.11

To my family, for their support
and patience.

Acknowledgments

Firstly, I would like to thank my family for all the patience with me throughout these two years. To my mom, for all the jokes and support. To my father, for always motivating me and suffering for Fluminense together. To my brother, for the companionship, advice and good times. To my cats Maia and Sol for all the love and bites.

To my advisor José Roberto Moraes d'Almeida for the patience, for sharing his knowledge and helping me since my undergraduate studies at Rio de Janeiro State University. He was also important in my personal development by providing opportunities to participate at conferences during my master's degree. I could not have asked for a better advisor.

To Prof. Larry Howell from Brigham Young University for collaborating with me during the making of this work. His suggestions and advice were of extreme help.

To Ana Beatriz, for all the love and support she has given me since we met. Her willpower motivated me to continue studying, restart personal projects and pursue my dreams. To Valéria and Reinaldo, for all the support and for accepting me so well in their family.

To my UERJ friends, Caio, Douglas, Eber, Giulia, Orlando, Peterson and Richard, for all the help and happy moments. A special thanks to Eber Dantas for the help and advice in the making of this work.

To professor Daniel Carlos Taissum Cardoso and all those who participated in the Petrobras project for the great teamwork and shared knowledge. A special thanks to Bruno and Jessé for helping me with the aged samples.

To Ayrton Pereira for helping me during these two years and for assisting me in the making of the colorimetric tests.

To Petrobras for the financial support during my study and opportunity to be part of an excellent research project.

To PUC-Rio for providing excellent facilities to perform high-level research.

To those who directly or indirectly contributed to the development of this work.

Finally, as this work was developed during the COVID-19 pandemic, I would like to acknowledge all health professionals and workers in general who fought and gave their lives battling against it. And to pay my respects to those who perished or lost loved ones during this horrible time.

This study was financed in part by the Coordenação de Aperfeiçoamento de Pessoal de Nível Superior - Brasil (CAPES) - Finance Code 001.

Abstract

Santos, Lucas Ferreira Lima dos; d'Almeida, José Roberto Moraes (Advisor). **Mechanical performance of an ortho-planar spring compliant mechanism after aging tests**. Rio de Janeiro, 2021. 101p. Dissertação de mestrado – Departamento de Engenharia Química e de Materiais, Pontifícia Universidade Católica do Rio de Janeiro.

In contrast to traditional mechanisms, a compliant mechanism relies on the deflection of its flexible members to generate motion, while presenting advantages such as no need for lubrication and easier assembly. An ortho-planar spring (OPS) compliant mechanism was analyzed in this work and its mechanical performance after hygrothermal and ultraviolet radiation aging tests was studied. The aging analysis performed here addresses the performance of compliant mechanisms after aging processes that can help in the design of future compliant mechanisms. ASTM D638 tensile test type I samples were also subjected to aging to serve as a comparison for OPS samples. The samples were subjected to three different types of aging conditions, namely water immersion, oil immersion and ultraviolet radiation. The liquid immersion aging tests were performed in three temperature levels: room temperature, 50°C and 70°C. In general, tensile samples showed significant statistical changes in Young's modulus and elongation at break, while OPS samples did not present considerable statistical change in any aging condition, which indicate that the mechanical properties and elastic capabilities of OPS samples were not affected by aging processes. Although more testing with the specific materials, environment, and exposure time would be required to verify its use in a specific application, the findings of this study suggest that compliant mechanisms show promise for use in applications where aging is a concern, and their life is expected to be within the limits of this aging study.

Keywords

Compliant mechanisms; Hygrothermal aging; UV aging; Ortho-planar spring; Additive manufacturing;

Resumo

Santos, Lucas Ferreira Lima dos; d'Almeida, José Roberto Moraes. **Comportamento mecânico de um mecanismo flexível de mola orto-planar após envelhecimentos**. Rio de Janeiro, 2021. 101p. Dissertação de Mestrado – Departamento de Engenharia Química e de Materiais, Pontifícia Universidade Católica do Rio de Janeiro.

Ao contrário dos mecanismos tradicionais, um mecanismo flexível conta com a deflexão de seus membros flexíveis para gerar movimento, ao mesmo tempo que apresenta vantagens como a desnecessidade de lubrificação e uma montagem mais fácil. Um mecanismo flexível de mola orto-planar foi analisado neste trabalho e seu desempenho mecânico após testes de envelhecimentos higrotérmicos e com radiação ultravioleta foram estudados. A análise do envelhecimento aqui realizada aborda o desempenho de mecanismos flexíveis após processos de envelhecimentos que pdoe ajudar no desenvolvimento de futuros mecanismos flexíveis. Amostras de tração ASTM D638 tipo I também foram submetidas aos envelhecimentos para servir de comparação para as amostras de mola orto-planar. As amostras foram submetidas a três tipos diferentes de envelhecimento, a saber: imersão em água, imersão em óleo e radiação ultravioleta. Os testes de envelhecimento por imersão em líquido foram realizados em três níveis de temperaturas: temperatura ambiente, 50°C e 70°C. Em geral, as amostras de tração mostraram mudanças estatísticas significativas no módulo de Young e no deformação na ruptura, enquanto as amostras de mola orto-planar não apresentaram alterações estatísticas importantes em nenhuma condição de envelhecimento, o que indica que as propriedades mecânicas e capacidades elásticas dos mecanismos não foram afetadas pelos processos de envelhecimento. Embora mais testes com os materiais específicos, ambiente e tempo de exposição sejam necessários para verificar o uso em uma aplicação específica, os resultados deste estudo sugerem que os mecanismos flexíveis mostram a promessa de uso em aplicações onde o envelhecimento é uma preocupação e sua vida é esperada estar dentro dos limites deste estudo de envelhecimento.

Palavras-chave

Mecanismos flexíveis; Envelhecimento higrotermal; Envelhecimento com UV; Mola orto-planar; Manufatura aditiva.

Table of contents

List of figures

List of tables

List of Abreviations

3D	Three-dimensional
3DP	Three-dimensional printing
ABS	Acrylonytrile butadiene styrene
AM	Additive manufacturing
AR	As received
ASTM	American Society for Testing and Materials
BC	Boundary condition
CBCM	Chained beam constraint model
CI	Carbonyl index
CM	Compliant mechanism
DLP	Digital light processing
FACT	Freedom, actuation and constraint topologies
FDM	Fused deposition modeling
FFM	Fused filament fabrication
FEA	Finite element analysis
FM	Flexible member
FML	Flexible member length
FTIR	Fourier transform infrared spectroscopy
HDPE	High-density polyethylene
LOM	Laminated object manufacturing
MFR	Melt flow rate
OI	Oil immersion
OI-RT	Oil immersion at room temperature
OI-50	Oil immersion at 50°C
OI-70	Oil immersion at 70°C
OPS	Ortho-planar spring
PA	Polyamide
PC	Polycarbonate
PLA	Polylactic acid
PRBM	Pseudo-Rigid-Body Model
RH	Relative humidity
RT	Room temperature
SLS	Selective laser sintering

TS	Tensile specimen
UV	Ultraviolet radiation
WI	Water immersion
WI-RT	Water immersion at room temperature
WI-50	Water immersion at 50°C
WI-70	Water immersion at 70°C

List of Symbols

δ	Displacement
ΔE	Difference in color
ΔL^*	Difference of L* of two points
Δa^*	Difference of a* of two points
Δb^*	Difference of b* of two points
γ	Characteristic radius factor
Θ	Pseudo-rigid-body angle
°C	Degree Celsius
a*	Value in the red/green axis in the color scale
b*	value in the yellow/blue axis in the color scale
cm	Centimeter
E	Young's modulus
F	Force
g	Gram
HU	Hazen unit
I	Moment of inertia
k	Torsional spring constant
K_Θ	Stiffness coefficient
L*	Coordinate that defines the luminosity in the color scale
m^3	Cubic meter
mg	Miligram
mho	Electrical conductivity measurement unit
mm	Millimeter
MJ	MegaJoules
MPa	MegaPascal
L	Length of the flexible element
pH	Potential of hydrogen
r	Length of rigid link between two torsional elements
T	Torque at each rotational spring
T_g	Glass-transition temperature
W	Watts

I would rather have questions that can't be answered than answers that can't be questioned.

Richard Feynman

1
Introduction

Traditional mechanisms are composed of rigid parts that are connected by pins and joints to generate motion and/or torque from one link to the others [1]. On the other hand, a compliant mechanism (CM) generate motion by the deflection of its flexible members [2]. Although several modern applications are constantly being developed using CMs, one of their first uses in mankind history dates from some thousand years ago with hunting bows, while in nature the use of compliance can be seen, for example, in bee wings, fishes and tree branches [2].

Polymeric materials are often used to produce CMs due to their mechanical and elastic properties. Although polymers do not suffer from corrosion, they can present mechanical and chemical deterioration after some period of exposure to aging conditions, such as ultraviolet radiation (UV), water humidity, high temperature and others [3–5].

UV radiation usually affect polymers by causing chemical degradation, which affect the original color of the material [6], and formation of microcracks that reduce the ductility potential [3]. Hygrothermal conditions such as water and oil immersion combine the aging effect of the liquid and temperature, being more aggressive as temperature increases [7, 8]. The damage related to the liquid depends on the polymer under aging and its affinity with the liquid, once after absorption of the moisture, this will start inducing chemical changes that will affect the physical [9] and mechanical properties [10]. As CMs are carefully designed to attend a specific application, a change in their performance can be critical. Thus, the study of the effect of aging in these mechanisms becomes essential. The aging conditions of ultraviolet radiation, water immersion and oil immersion were analyzed and the samples of this work submitted to them.

An ortho-planar spring, Fig. 1.1[1], is a compliant mechanism, which has characteristics such as compact geometry in its compressed or uncompressed position and can be manufactured from a single piece of material. It was already used in a valve application [11]. Here, a 3D printed ortho-

[1]Images were taken from the Thingverse profile of the Brigham Young University Compliant Mechanisms Research group. The images can be accessed by the following address: www.thingiverse.com/thing:3007261.

planar spring compliant mechanism specimen made of acrylonitrile butadiene styrene (ABS) was selected to study the effect of aging conditions on its mechanical performance. Three different aging conditions were chosen: UV, water immersion (room temperature, 50°C and 70°C) and oil immersion (room temperature, 50°C and 70°C). As the degradation process is accelerated by the increase of temperature, these three different temperatures levels were used to evaluate the mechanical performance changes observed on the compliant mechanism. An aging analysis of a traditional ASTM D638 tensile test type I specimen was also carried out to serve as a comparison base for the compliant mechanism, once it is made of the same fabrication process and material.

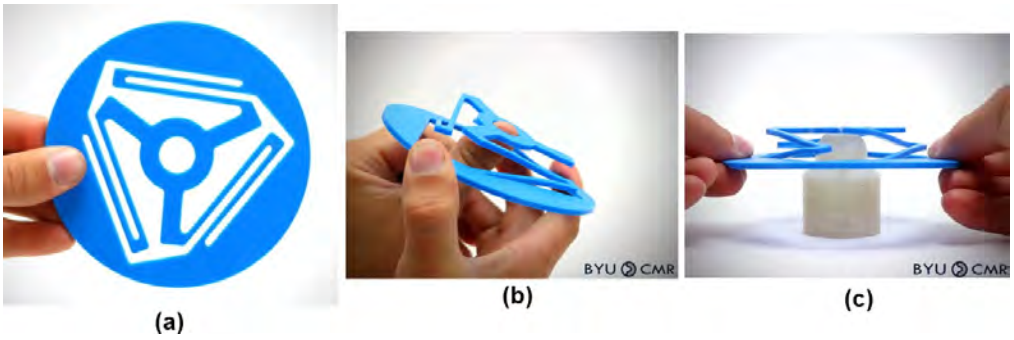

Figure 1.1: Ortho-planar spring in its (a) uncompressed and (b),(c) compressed states.

Colorimetric tests were performed in all samples of this work to evaluate how a certain condition affects the natural color of a sample, which is usually an indication of the degree of chemical degradation in a sample. A color change can be directly related to a chemical degradation process inside the material. Therefore, it is interesting to know which conditions cause the most significant changes.

Several studies can be found in the literature dedicated to the analysis and synthesis of compliant mechanisms, but the author could not find works related to the study of the performance of CMs when exposed to some kind of aging condition in the literature, which is of ultimate importance and a motivation for this work. By knowing how a mechanism reacts to a certain aging condition, it is possible to design it appropriately so that the mechanism can withstand this condition for a greater amount of time.

2
Literature review

2.1
Compliant mechanisms

A mechanical device composed by rigid links connected by joints with one of the links fixed can be called a mechanism, whose function is to transform motion and/or torque from one link to the others [1].

A compliant mechanism is different from conventional rigid mechanisms. While the latter depends on movable joints to have mobility, the former is able to use the deflection of its flexible members [2]. Usually, a CM requires fewer parts to accomplish the same tasks as the traditional mechanisms and present interesting advantages, as the significant cost reduction, once the assembly is reduced, less stocking of components and simple manufacturing [12]. It can also be pointed out that CMs present low weight and eliminate the need for lubrication, which is an improvement for many applications [13].

In one of the compliant mechanism design lectures[1] of Jonathan Hopkins, professor from University of California Los Angeles, he preferred to use the term limitations instead of disadvantages when talking about CMs. The reason is because most current issues can be overcome in the future with technological advancements. The most important limitation is related to design and analysis, once it includes non-linear deflections and increase the difficulty of the design. This was one of the reasons why CMs took so long to be more present in mechanical designs, but with new developments in the field of finite element analysis, topology optimization and 3D printing, complex CMs can be easier designed and fabricated. Other limitations include energy storage disadvantages, fatigue and limited deflection range. According to prof. Hopkins, there are means to get around those three issues and new solutions continue to appear.

Examples of CMs range from very basic applications, like an Ethernet cable connector plug, used for network cabling to highly complex ones, such as the mechanism presented by Gou et al. [14], Figure 2.1. The author studied

[1]The FACTs of Mechanical Design. "Compliant Mechanisms Lecture 1 Part 3". Youtube, March 22, 2021. Available at: `https://youtu.be/h8uSjfbU0hg`. Accessed on May 3rd 2021.

the design parameters of a compliant mechanism that presents eight stable equilibrium positions.

Figure 2.1: Compliant mechanism studied by Gou et al. [14] with eight stable equilibrium positions.

In the past, humanity always favored rigid mechanisms as they seemed more reliable and durable. With the development of new technologies and materials, it is now possible to create trailblazing mechanisms with reduced weight, no lubrication and more precise. Lately, many high-precision based applications are making use of CMs [15–17]. Other studies focus on implementations in a diversity of areas, namely, medicine [18, 19], automotive [20, 21] and robotics [22–24].

CMs can be manufactured from lots of different materials. Polymers are usually the most used type of material, but titanium [25], steel [26, 27] and composite materials [28] were already employed. This diversity is important, once you can associate the characteristics of a certain material with the advantages of CMs.

2.1.1 Synthesis

The synthesis of compliant mechanisms can be performed by different methods. The Pseudo-Rigid Body Model (PRBM) [29], FACT (Freedom, Actuation and Constraint Topologies) [30] and Topology Optimization [31, 32] are some of the most popular ones. There are also methods to evaluate the mechanical behavior of the mechanisms, such as the Chained Beam Constraint Model (CBCM) [33] and finite element analysis (FEA) [34]. The latter can be performed directly with the aid of a commercial software or programming.

With the project done, the compliant mechanism can usually be manufactured by 3D printing techniques. In Item 2.2, details concerning additive manufacturing and some of its techniques will be discussed.

In the next section, the PRBM method will be further discussed, as this is the most relevant for this work.

2.1.1.1 Pseudo-Rigid-Body Model

The Pseudo-Rigid-Body Model (PRBM) [35] was created with the purpose of modeling flexible members of compliant mechanisms that undergo large and nonlinear deflections by using rigid-body components that have similar force-deflection characteristics. With the insertion of pin joints to model motion and springs to model flexible members stiffness, this method creates a connection between rigid-body and compliant mechanism theories.

Fixed-guided segments are the base for the modeling of ortho-planar springs, so the focus of this section will be on these kind of segments, once the PRBM can be used to model a variety of mechanisms and a complete discussion would surpass the objectives of this work.

The PRBM of a fixed-guided segment is shown in Fig. 2.2, composed of two rotational springs.

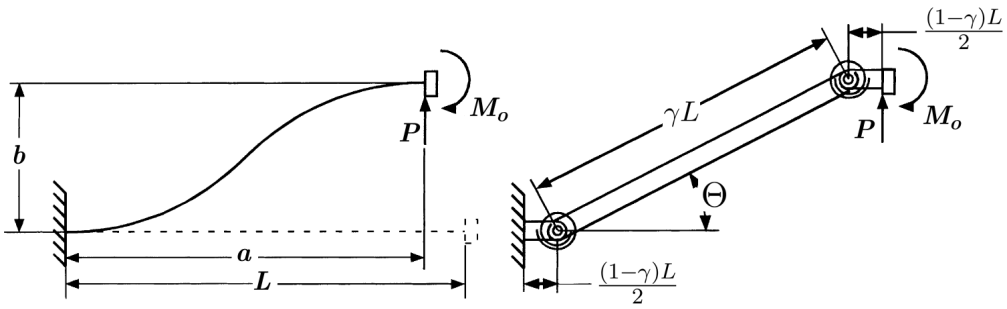

Figure 2.2: Pseudo-rigid-body model of a fixed guided segment. Figure adapted from Parise et al. [11].

The rigid link between the two rotational elements have length r, Eq. (2-1), and the torsional springs have torsional spring constant of k, Eq. (2-2), where γ is the characteristic radius factor (usually $\gamma \approx 0.85$) [2], L is the length of the flexible segment, K_Θ is the stiffness coefficient (usually $K_\Theta \approx 2.65$) [35], E is the Young's modulus of the material of the spring and I is the moment of inertia.

$$r = \gamma L \tag{2-1}$$

$$k = 2\gamma K_\Theta \frac{EI}{L} \tag{2-2}$$

The end coordinates of the segment, point (a,b), are

$$a = L[1 - \gamma(1 - \cos\Theta)] \tag{2-3}$$

and

$$b = \gamma L \sin\Theta \ , \tag{2-4}$$

where Θ is the pseudo-rigid-body angle in radians. Finally, the moment at each rotational spring can be calculated with the expression

$$T = k\Theta \ . \tag{2-5}$$

2.1.2 Ortho-planar spring

Ortho-planar spring (OPS) is a device that can be fabricated in or compressed to a single plane [11]. Belleville disc springs, volute springs and spider springs are some types of OPS and can be seen in Fig. 2.3.

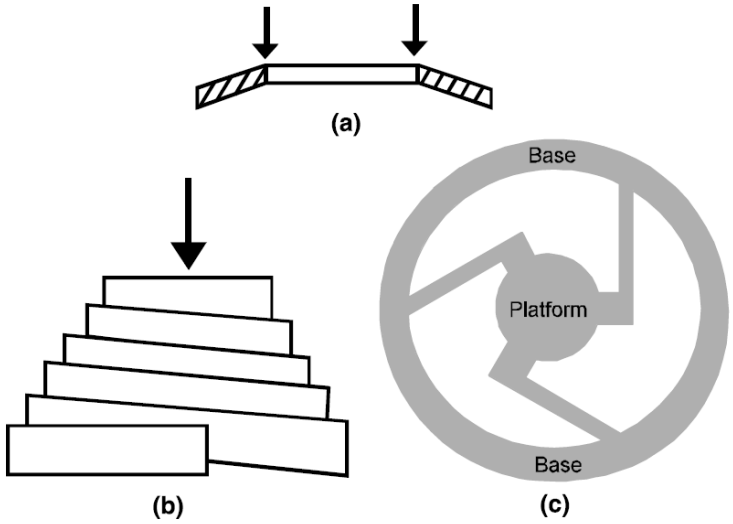

Figure 2.3: Three types of ortho-planar springs [11]: (a) cross-section of a Belleville disc springs, (b) volute springs and (c) spider springs.

An OPS has compact geometry in its compressed or uncompressed positions, which makes them suitable for applications with limited size. They can also be manufactured from a single piece of material, being easier to manufacture.

On the other hand, these types of OPS present some important disadvantages. The volute and spider springs generate a rotation during operation, which forces the attached surface to rotate together with the spring. Depending on the geometry of the spring, more clearance is required to avoid contact with adjacent structures. The spider spring presents a reduced total

possible deflection and fatigue life, once the rotation of the legs adds torsional stress to the members [11].

Therefore, Parise et al. [11] developed a new design of an OPS that overcomes these disadvantages. It has the advantage of not presenting rotation in any of the three directions (x, y and z) during deflection. The mechanism has two possible types: radial-leg design and side-leg design as can be seen in Fig. 2.4. Both designs are unstable when composed of two legs, i.e., they allow motion in the x or y directions, but become more stable with increased number of legs. As a rule of thumb, designs of the mechanism with an odd number of legs greater or equal to three tend to be more stable.

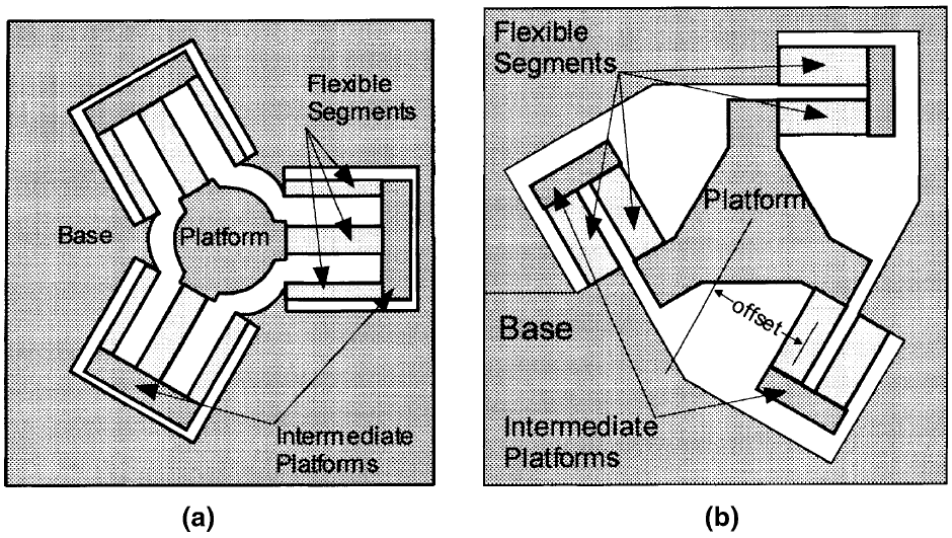

Figure 2.4: Two possible types for the OPS presented by Parise et al. [11]: (a) radial-leg design and (b) side-leg design.

The mechanism and some important terms of the OPS geometry that will be used throughout this work are shown in Fig. 2.5. The union of an intermediate platform and its connected flexible members is called a leg of the mechanism. Thus, the mechanism of this work contains three legs, six flexible members and 3 intermediate platforms.

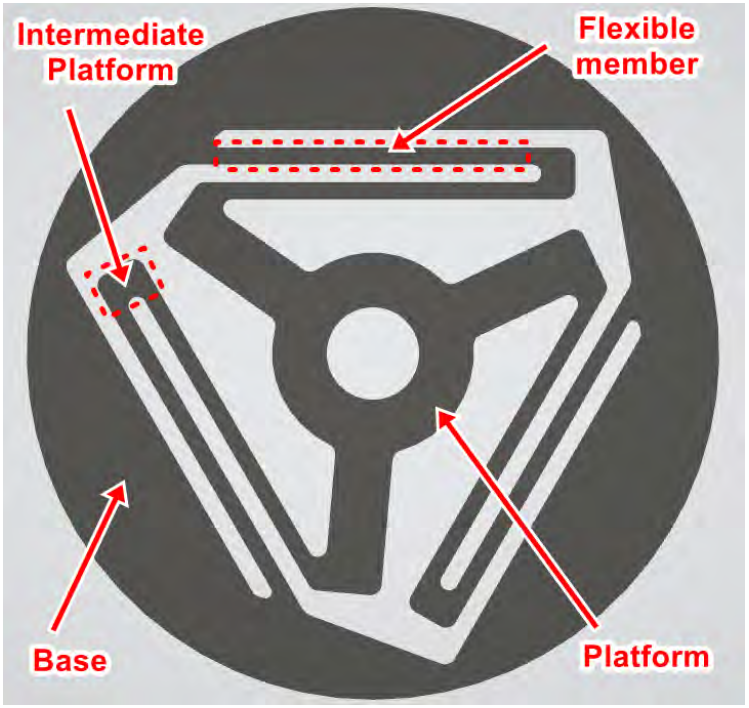

Figure 2.5: Geometry terms of the ortho-planar spring specimen.

2.2 Additive manufacturing

Additive manufacturing (AM), also known as 3D printing, is the process of creating materials layer-by-layer until the product is finished [36]. Over the past decade, the global market of 3D printed materials experienced an enormous increase, going from $5 billions in 2015 to a expectancy of $41 billions in 2027 [37]. With future advances on this field, this revenue tends to continue increasing.

2.2.1 Fabrication methods

There are several fabrication methods in additive manufacturing, namely, Fused Deposition Modeling (FDM), Stereolithography (SLA), Digital Light Processing (DLP), Selective Laser Sintering (SLS), Three-Dimensional Printing (3DP), Laminated Object Manufacturing (LOM) and Polyjet Technology [38].

Independently of the chosen method, an initial step is followed. Firstly, the desired product needs to be modeled in a 3D software, e.g., Solidworks, 3ds Max or Inventor. When finished, it must be saved as 3D file format that can be read by the printer (usually STL format). Finally, the file is provided to the printer's software and then it is sliced in multiple layers [38].

FDM and SLS techniques play an important role in this work, as the samples used for testing were made with FDM and some works in the literature concerning compliant mechanism make use of SLS [34,39,40]. In the next items, these two methods will be discussed.

2.2.1.1 Fused Deposition Modeling

Fused Deposition Modeling (FDM) is the trademarked term for the Fused Filament Fabrication (FFM) process. The method consists in the extrusion of a melted material, usually a polymeric filament, from a nozzle. The nozzle follows pre-determined paths created by the 3D printer, so that the final product is modeled layer-by-layer. In Figure 2.6, the FDM process is presented, where the extrusion head only works in the x-axis and y-axis while a vertical support moves in the z-axis when a layer is done. There are also printers that have a fixed base with the extrusion head moving in all directions.

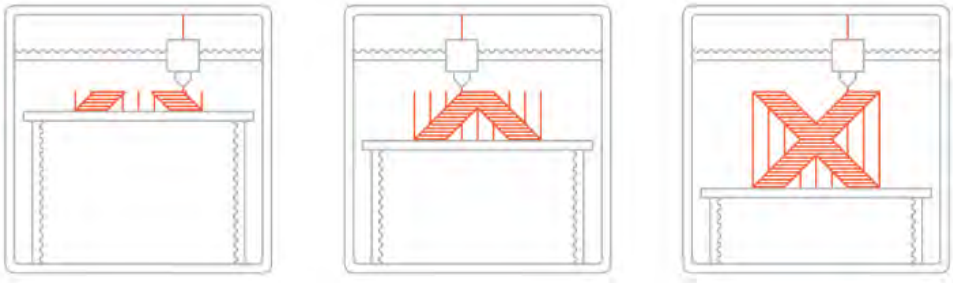

Figure 2.6: FDM printing process [41].

The FDM process is the simplest of all AM fabrication methods. Firstly, the nozzle is heated until it reaches the process temperature. Then, the filament is directed to the extrusion head and then melted in the nozzle. The 3D printing process is initiated and the filament is deposited following the pre-determined path set by the printer to fill the layers until the piece is finished. For some parts, a support structure will be needed. In Figure 2.6, the printer had to make vertical supports in order to print the diagonals of the piece. It is usually used a different material in order to print the support structures, so in this case the extrusion head will have 2 filaments attached to it, as can be seen in Figure 2.7.

In the printing configuration step, it is possible to define the infill percentage of the part. When the percentage is lower than 100%, there will be non-filled areas inside the piece. Most printers come with a set of pre-defined infill patterns that the user can choose. In Figure 2.8, four infill patterns are shown: rectangular, triangular, wiggle and honeycomb, respectively. The black thick line represents the outer shell of the part. The pattern is important if the

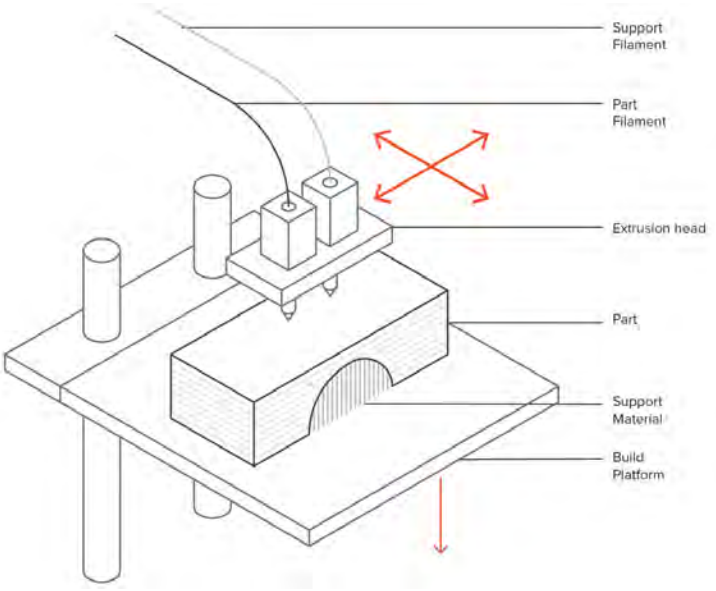

Figure 2.7: Support structures in the FDM printing process [41].

product being printed requires special attention to mechanical performance, once it affects the mechanical properties of the product. The honeycomb pattern, for example, is more isotropic than the wiggle pattern, once it is symmetric, thus, presenting the same resistance to tension or compression in the x-axis and y-axis.

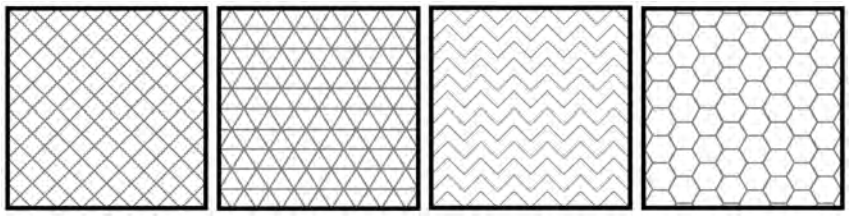

Figure 2.8: Four examples of infill patterns in FDM printing: rectangular, triangular, wiggle and honeycomb [42].

A common problem of FDM printing is the warping of printed layers. Some possible causes are the contraction of layers after cooling and the non-uniform temperature distribution between the support base and the material, resulting in deformation of the part [43]. The printer base is usually pre-heated before the start of the printing process to avoid this issue. In Figure 2.9, one can see a warped surface of a printed part by FDM.

Wang et al. [44] investigated the effect of FDM process parameters in the mechanical properties of uniaxial tensile specimens made of polylactic acid (PLA). Specimens with 100% fill rate presented 2.7x larger tensile strength than the ones printed with 20% fill rate (53.66 MPa versus 20.04 MPa). The printing angle of the layers, Figure 2.10, is also an important parameter. Specimens with 90 degrees (parallel to test direction) presented 1.95x and

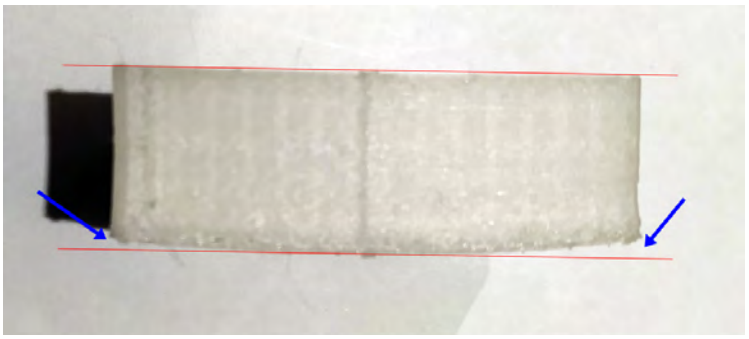

Figure 2.9: An example of warping in a FDM printed part. The base is clearly not straight (as it should be) and the top is flatter. The red lines indicate how the surfaces should be aligned and the blue arrows point out the warped surface.

4x larger values for tensile strength and elongation at break, respectively, compared to those with zero degrees (perpendicular to test direction). The layer thickness also have an impact in the mechanical response. For higher values of the thickness, the properties tend to decrease.

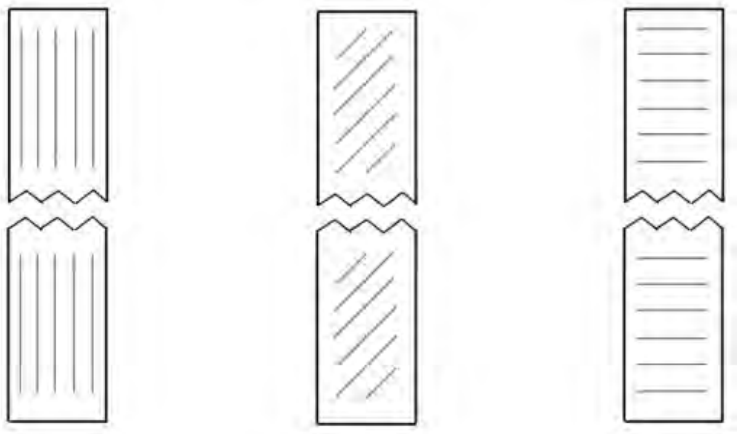

Figure 2.10: Different printing angles for a FDM printed part. Figure adapted from reference [45].

The FDM process presents many advantages, namely, low manufacturing cost, wide range of materials to print and is an extremely simple process. It is also safe and produces minimum waste [43]. On the other hand, FDM parts present low dimensional accuracy, thus, it is not recommended for highly-detailed objects. Finished parts tend to have visible layers, which can be a downside if aesthetics is important.

2.2.1.2 Selective Laser Sintering

Selective Laser Sintering (SLS) is the process where the part is produced by the action of a laser beam in a powder reservoir. Firstly, the main powder

storage is heated up to the process temperature. Then, a single layer of powder is deposited by a recoater. The laser beam scans the powder surface in order to sinter the current layer at the locations where the presence of material was planned. After the scan, the building platform moves down one layer height and then a new layer of powder is added, being distributed by the recoater. This whole procedure is repeated until the final product is done. In Figure 2.11, a schematic diagram of the SLS process is presented.

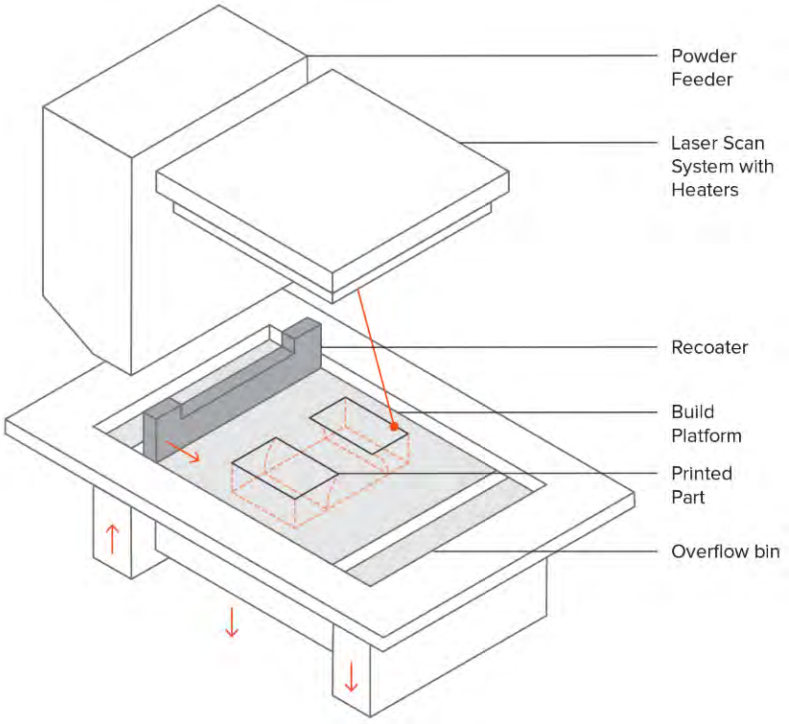

Figure 2.11: Schematic diagram of the SLS printing process [46].

After all the layers are done, the finished part is removed from inside the block of powder. The unsintered powder is usually recycled to the next printing. Dotchev [47] investigated the change of the melt flow rate (MFR) of unsintered powder in the SLS process, i.e., the ability of a material to flow in a limited interval of time [48]. It was found out that the MFR decreases significantly for higher process temperatures and longer exposure times. This drop in the MFR means that the viscosity of the material increased. Feng et al. [49] also reported an important deterioration on the MFR of unsintered powder, but the recycled polyamide 12 (PA 12) powder, when used in injection molding, presented mechanical properties only slightly decreased when compared to fresh PA 12. Transforming the recycled powder to pellets before the injection molding created specimens with higher MFR than the ones made with recycled powder, but the MFR was still way smaller (65%) than the ones made with virgin PA 12. Zarringhalam et al. [50] compared the mechanical performance of specimens

made of virgin powder and used powder. The latter presented enhanced tensile strength and elongation at break and both had similar Young's modulus. This can be explained by the increased molecular weight of used powder due to additional cross-linking [51].

When looking at SLS process parameters, some of them can contribute for making prototypes with different mechanical properties. Majewski et al. [52] tested different settings of a SLS machine, including laser power, to compare the performance of Nylon parts. The analysis had as hypothesis that the amount of unmelted particles present in the microstructure interfered in the mechanical response. By differential scanning calorimetry tests, it was possible to visualize the peaks from melted regions and unmelted ones. Then, after printing with the new machine parameters and testing, a correlation between the parameters, peak heights and amount of unmelted particles was established. Parts with higher amount of unmelted particles presented inferior mechanical properties in all cases. Ajoku et al. [53] analyzed the effect of build orientation on SLS printing. Specimens printed in the x-axis presented the best properties, while the ones printed in the z-axis had the worst performance. Ajoku also investigated the end-of-vector effect, i.e., the laser power is stronger at the beginning of the scan and then it stabilizes. The y-axis specimens showed improved flexural properties due to this effect, once the printed width of the part was shorter and it caused greater sintering and more densification.

The SLS process presents some advantages, once it does not require support structures (FDM requires) and it can be more cost-effective when producing several prototypes on the same batch. The reason for not requiring support is because the unsintered powder of the previous layer acts as the support for the next one. On the other hand, the cost of SLS printing is high due to expensive heating sources [54].

2.2.2 Post-processing

After the 3D printing process, some parts require further work in order to achieve a satisfactory level of mechanical property or simply to improve the aesthetics. Post-processing in FDM is commonly performed to remove burrs or remove supports from finished parts, but there are other procedures that can also be applied, namely, sanding, cold welding, gap filling, polishing, priming and painting, vapor smoothing, dipping, epoxy coating and metal plating [55]. Some post-processing methods for SLS printed parts include vibro polish, dyeing, painting and lacquering, watertightness and metal plating [56].

Zhang et al. [57] applied microwave irradiation on FDM specimens

reinforced with carbon nanotubes. One minute of irradiation was enough to improve the tensile strength and flexural strength in 30% and 13.1%, respectively. This enhancement in a short-term exposure can be explained by the fact that the carbon nanotubes present a remarkable response to microwave irradiation, which makes the layers of polymers fuse locally.

Shaw and Dirven [58] found out that the level of porosity in SLS parts can be up to 30%. They associated this characteristic with the weak mechanical properties of parts made by this method. The authors suggested that a resin impregnation procedure could be applied in order to fill those voids and enhance the mechanical response of SLS printed parts.

2.3 Acrylonitrile butadiene styrene

The acrylonitrile butadiene styrene (ABS) polymer is a thermoplastic terpolymer, which has many practical applications, such as wheels, gears, refrigerator liners, pipe, sporting goods and others due to its toughness and rigidity [59]. ABS is usually formed by the combination of three monomers: acrylonitrile, butadiene and styrene. An scheme of the ABS monomer is shown in Fig. 2.12. Each of the three monomers contributes with the following properties to the final polymer [59]:

- Acrylonitrile - Chemical resistance, heat resistance and high strength.
- Butadiene - Toughness, impact strength and low-temperature property retention.
- Styrene - Rigidity, surface appearance (gloss) and processability.

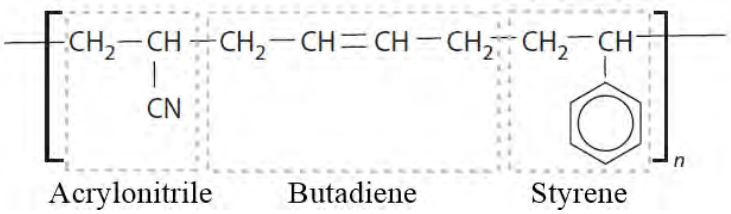

Figure 2.12: Scheme of an Acrylonitrile Butadiene Styrene (ABS) monomer. Figure adapted from Chanda [59].

Other monomers can be added to the fabrication process for specific usage, e.g., fumaronitrile and α-methylstyrene allow high temperature application for ABS and methyl methacrylate and N-phenylmaleimide add the characteristic of high gloss to ABS [60].

According to Chanda [59], ABS has adequate chemical resistance, being not significantly affected by water, but has poor resistance to ultraviolet (UV)

radiation. This is an important information for the purposes of this work, once the aging by water and UV are two of the three aging conditions that the specimens were subjected to.

2.4 Degradation of polymers

It is well known and vastly studied that the main cause for the degradation of polymers is by its exposition to environmental agents [3–6, 10, 61–67]. According to ASTM D883 (Standard terminology relating to plastics) [68], "aging is the effect on materials of exposure to an environment for an interval of time". The consequences of this process are usually chemical degradation of the polymer structure, deterioration of mechanical and physical properties and changes in its color.

In this work, the specimens will be exposed to temperature, water immersion and UV radiation. Thus, in the next items, it will be discussed the effects reported in the literature of these aging conditions.

2.4.1 Hygrothermal aging

Hygrothermal aging is related to the combined aging effect of liquid and temperature. Polymers tend to present different behaviors depending on the temperature it is exposed to. In general, the degradation process is accelerated with the increase of temperature [7, 8]. When the liquid used is water, this process is known as hydrothermal aging.

When immersed in water or exposed to an environment of significant relative humidity, the polymers absorb and adsorb water, which increases its weight, changes its chemical structure and degrades the mechanical properties [10, 69]. The immersion in water can also cause discoloration of the polymer matrix in composites [65,66]. Decrease of the glass-transition temperature (T_g) at different hydrothermal conditions and exposure times was also reported in the literature [9,70]. Yu et al. [71] studied the effect of moisture absorption on polyurethane foams and one of the results was the change in the T_g for varying levels of humidity and temperatures, Figure 2.13.

Kajorncheappunngam et al. [72] investigated the variation of some mechanical properties of an epoxy resin under different aging conditions for 1, 3 and 5 months of exposure. The samples exposed to distilled water presented an enhancement of mechanical properties in the first month, mainly due to the fact that the polymer was not fully cured. The curing of the aged samples was faster for the higher temperature condition (60°C). After the polymer was

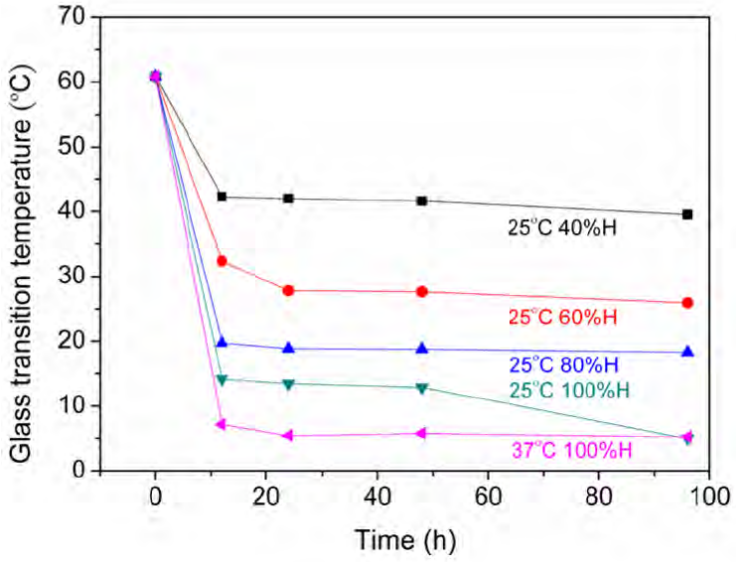

Figure 2.13: Changes in the glass-transition temperature of a polyurethane foam exposed to different humidity levels (H) and two different temperatures [71].

fully cured, a decrease of mechanical properties was observed in samples aged for 3 and 5 months.

The effects of aging with water are not equal to all polymers, once the chemical structures are different and can contain polar or nonpolar groups, facilitating or not the absorption of water. Polymers with high hydrophilicity tend to present swelling and plasticization, while polymers with low to moderate hydrophilicity suffer more to hydrolysis, which leads to cracking [73].

As some polymers can be exposed to oil, as in oil pipes, some studies investigate its effect in the mechanical performance of those polymers. Amaral [74] studied the effect of lubricant oil in color and mechanical properties of polyamide 12 (PA 12) and high-density polyethylene (HDPE). The most significant changes, regarding mechanical properties, were noticed in the Young's modulus, which decreased by 11.7% and 20.4% in PA 12 and HDPE, respectively. There was also a difference between polymer color before and after aging. Both PA 12 and HDPE tended to the same hue, once the liquid used was the same.

Pereira et al. [75] analyzed the effect of diesel oil and gasoline in the creep behavior of HDPE. Aged samples showed increased creep rates, especially the diesel oil aged specimens, which caused shorter lifetimes of these materials. They also noticed an increase in material flexibility, once there was affinity between diesel oil and gasoline with HDPE functional groups, causing plasticization.

Another interesting study was conducted by Hernández and d'Almeida

[76]. They investigated the effect of oil and pressure in the mechanical properties of PA 12. At room temperature and atmospheric pressure, no significant changes were caused by the agents and the color of specimens remained unaltered. The aging of specimens in 70°C and pressures of 1 atm and 17 atm were responsible for absorption of oil, evidenced by the change in color of the samples. Nonetheless, no significant chemical structure changes were noticed. The authors conclude saying that PA 12 is an interesting material for industry, once it shows satisfying resistance to oil aging in varied pressures and temperatures.

The effect of temperature depends on its value and the material under aging. In general, higher temperatures only cause a faster reach of the saturation levels of moisture absorption [77, 78], once diffusion is a thermally activated process [79]. Therefore, lower temperatures take a longer time to reach the saturation level.

An exception for this behavior is when aging temperature is close to the materials T_g, which causes chemical changes in the polymer, allowing a higher value of moisture content [80, 81]. Plessix et al. [80] observed that aging temperatures near the material T_g causes plasticization, enabling increased absorption. Robert et al. [81] investigated this issue with composites and concluded that the material presented higher coefficient of thermal expansion This changed the density of free volumes and made the material more porous, which lead to a higher absorption capacity.

The hygrothermal aging, in sum, tends to decrease the mechanical properties of the polymeric materials under aging. It is possible that an initial increase in the properties is noticed due to the non-fully cured state of the material [72], but as aging time goes by, the properties tend to decrease significantly.

2.4.2 UV radiation aging

It is commonly known that the exposure to UV radiation affects the polymer surface, causing chemical degradation and noticeable change in its original color [6]. Studies often report the appearance of microcracks in polymers [4] and polymer matrix of composites [3] as consequence of UV exposure.

Kumar et al. [3] investigated the changes in laminate carbon fiber epoxy composites when exposed to UV radiation. Minor decrease in weight and significant change in color from black to dark green were reported. Optical micrographs showed formation of microcracks in the epoxy matrix, Figure

2.14, as a result of 500h of exposure to UV radiation. The author associated this with the photo-oxidation reactions induced by UV, which made the matrix excessively brittle due to increased crosslinking.

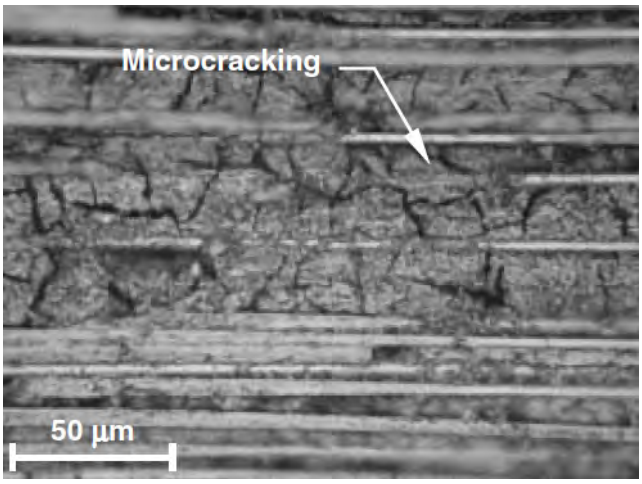

Figure 2.14: Optical micrograph of the carbon-fiber-epoxy composite, studied by Kumar et al. [3], after 500h of exposure to UV radiation.

Ghasemi-Kahrizsangi et al. [4] studied the effect of UV exposure to epoxy coatings with and without carbon black nanoparticles and observed several microcracks on the epoxy without the filler. Higher concentration of nanoparticles showed significant resistance to UV exposure.

Becerra and d'Almeida [6] analyzed the effect caused by UV exposure in HDPE samples. They performed the aging in tensile test specimens and concluded that the crystallinity decreased, once crosslinking was induced as consequence of the energy provided by UV radiation. This also contributed to an increase in the Young's modulus and yield strength.

Bociaga and Trzaskalska [82] investigated the effect of UV radiation on the gloss and color properties of injection moulded ABS samples. Three types of specimens with different coloring agents were compared to the not colored specimen. All samples presented a decrease of approximately 75% in gloss value, while the luminance value has increased, meaning that the samples began to fade and brighten. The authors associate the decrease of gloss value with the degradation of ABS amorphous structure.

In general, works that analyze UV aging in polymers often report similar damages caused to the materials. The degree of these effects will obviously vary depending on the polymeric material that is being used and also on the exposure time.

2.4.3 Degradation of ABS

Due to the wide range of polymers used nowadays, it is wrong to assume a general behavior after aging processes. Some polymers (e.g., epoxy) are more resistant to hydrothermal aging, while others (e.g., polyester) suffer from hydrolysis, which is the event of chemical bonds breakage induced by water molecules. In this item, the objective is to, with the aid of some literature works, understand the changes in ABS when subjected to aging environments.

Boldizar and Möller [83] analyzed the mechanical performance of ABS exposed to air at 90°C. The samples were tested in three different conditions: cycles of extrusion, where the samples were recycled after the testing, cycles of aging for 72h and the combined condition of extrusion and aging cycle, where the samples were tested after the extrusion and then after the aging. The combined condition degraded the material the most as evidenced by the measurement of oxidation induction temperature and melt volume-flow rate. Due to the aging processes, ABS presented an increase in the carbonyl groups (Fig. 2.15), which is something that can be partially reversible after an extrusion process. At last, the elongation at break of the samples decreased for the condition of only aging cycles and increased after extrusion cycles.

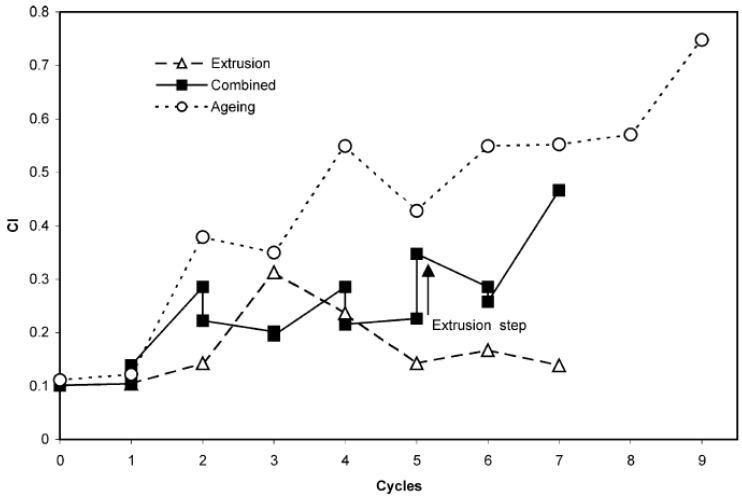

Figure 2.15: Carbonyl index (CI) of the ABS samples after cycles of the three conditions (extrusion, aging and combined) [83].

Fiorio et al. [84] investigated the effect of accelerated UV aging with temperature in the properties of ABS tensile test specimens before and after mechanical recycling. They observed that the tensile modulus increased in the aged specimens when compared to the as received and recycled samples. On the other hand, the strain at break was higher in the as received and recycled specimens and significantly lower in the aged samples. No relevant changes

were noticeable in the tensile strength specimens after aging and recycling processes. The authors conclude saying that ABS can be recycled for new plastic parts for use in applications that do not require toughness, once the aging and recycling reduce this property.

Li et al. [85] studied the changes of pure ABS and blends of ABS with polycarbonate (ABS/PC) submitted to UV radiation. Using Fourier transform infrared spectroscopy (FTIR) analysis, the authors observed that ABS samples presented increased absorbance in the region of alcohol and acid groups as the aging time increased (Fig. 2.16 (a)). It could also be observed that the aged ABS specimens presented the formation of carbonyl groups, Fig. 2.16 (b), while the unaged ones showed no absorbance from those groups. Moreover, the aged ABS samples began to lose the butadiene bands after aging, which could explain the increase of oxygen-containing groups (Fig. 2.16 (c)). Finally, when compared to the blend materials of ABS/PC, the latter possess higher photo-stability than ABS, which can be seen as a solution to increase UV resistance of pure ABS.

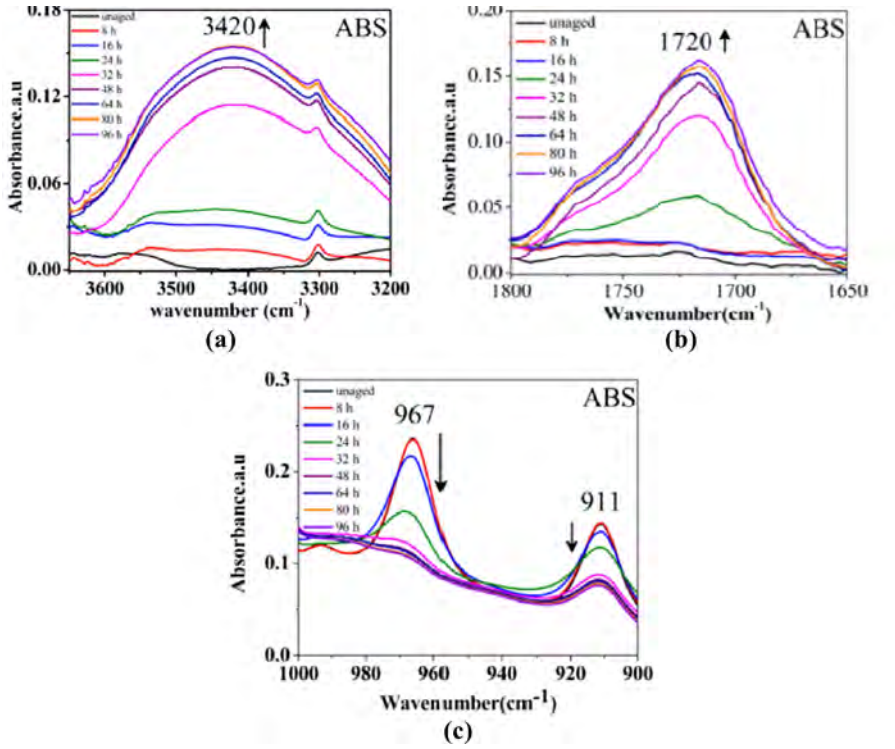

Figure 2.16: Chemical changes in pure ABS detected by FTIR analysis in the regions of (a) alcohol and acid groups, (b) carbonyl groups and (c) butadiene bands. This figure was made by grouping different figures of the work from Li et al. [85].

It is important to state that papers regarding hygrothermal aging of pure ABS samples are rare, which is also a motivation for this work. In Item 2.4.4,

a work that studied hygrothermal aging of a 3D printed ABS specimen will be discussed.

The presented literature works reported important changes on ABS behavior, e.g., carbonyl groups increase after aging [83, 85]. It was also shown that the UV resistance of pure ABS is poor, which is something to consider in applications. As shown in the work of Li et al. [85], this problem can be addressed by combining ABS with polycarbonate.

2.4.4 Aging effects on 3D printed polymers

The aging of polymers is vastly studied and their behavior after this processes is well-known, as discussed in previous items. On the other hand, the effects of aging in 3D printed polymers is not as investigated as in traditionally fabricated polymers, once 3D printing only started to popularize in the past decade. Thus, it becomes important to address this subject to a better understanding and comparison with this work.

Kakanuru and Pochiraju [86] investigated the effects of immersion in distilled water at 50°C on three materials: PLA, a composite of PLA with silicon carbide (SiC) and ABS printed polymers. The ABS samples showed no significant change in the ultimate tensile strength, an increase of 19% in the tensile failure strain and presented a decrease of 33% in the Young's modulus. In Fig. 2.17, it can be seen the difference between the mechanical performance of unaged (Dry) and aged (Wet) ABS samples. The authors were not able to test the PLA and PLA with SiC specimens after aging. The PLA samples were partially disintegrated and the PLA composites were excessively brittle.

Popescu et al. [87] analyzed the effect of natural aging (normal daylight changes) and multiple sterilizations on 3D printed ABS to reproduce usual conditions that medical instruments are exposed to in daily hospital processes. They evaluated the changes in mechanical performance of standard specimens through tensile and flexural tests, which showed no significant alteration after aging when compared to the unaged samples. The authors then state that 3D printed ABS can be used to produce medical instruments.

Goodridge et al. [88] compared the mechanical performance after aging of PA 12 specimens fabricated from laser sintering and injection moulding. One thing worth mentioning regarding this work is the fact that the authors used different materials in each fabrication method, which compromise an adequate comparison. Therefore, only the results of the printed samples will be discussed. The specimens were submitted to two aging conditions for 52 weeks: relative humidity of 50% (condition A) and immersion in water (condition B). An initial

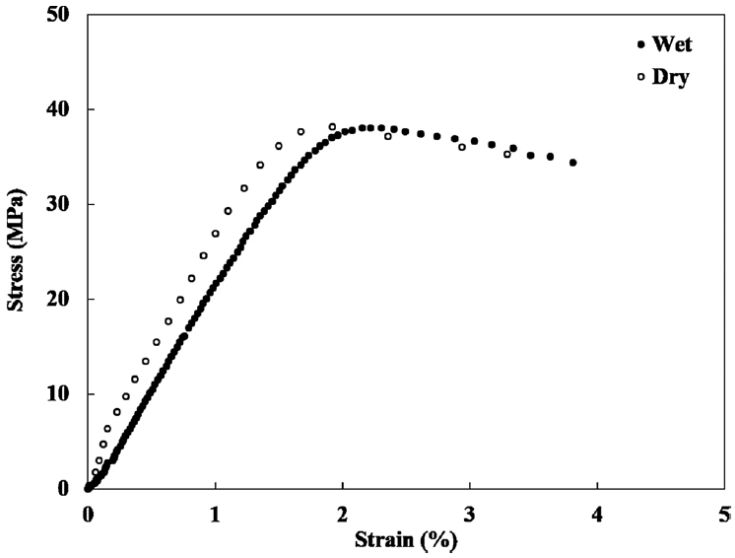

Figure 2.17: Stress-strain curves of the unaged (Dry) and aged (Wet) 3D printed ABS samples [86].

increase of the Young's modulus was noticed for both conditions. Then, samples from condition A remained at that increased level for the rest of the aging, while the ones from condition B presented a decrease. The ultimate tensile strength was also measured, being constant for specimens from condition A and lower for the ones from condition B. These results confirm that the aging is more aggressive for higher values of relative humidity and temperature, as discussed in Item 2.4.1.

The works mentioned above contribute to the discussion of aging in 3D printed polymers. As expected, those materials also suffer from exposure to aging environments. Differently from injection moulded samples, printed polymers have the peculiarities of presenting more voids and layer-to-layer imperfections, which makes them an interesting material to be studied.

3
Materials and methods

In this work, two types of specimens were used to study the effect of aging conditions in compliant mechanisms. The first one is an ortho-planar spring compliant mechanism, Fig. 3.1, that was introduced by Parise et al. [11] and is composed of 3 legs and 6 flexible members of length L and thickness T. The other one is a 3D printed ASTM D638 tensile type I specimen (TS) [89], Fig. 3.2, which will serve as a comparison for the analysis of the effect of aging. The measured dimensions of 3D printed OPS and tensile test samples can be found in Appendix A and Appendix B, respectively.

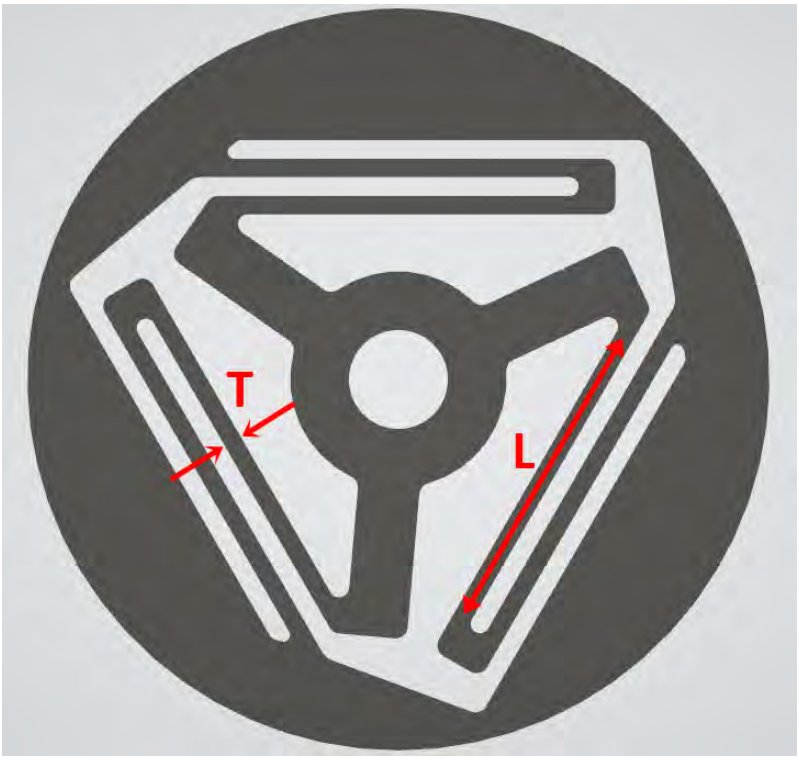

Figure 3.1: Geometry and dimensional parameters of the ortho-planar spring.

The experimental procedure can be summarized by the flowchart shown in Fig. 3.3. The aging conditions were the same for both specimens with 3 samples of each one being used in each condition, which results in a total of 48 samples, i.e., 24 for each specimen type.

To make the analysis simpler, the specimens conditions will be represented by symbols as follows: as received (AR), ultraviolet radiation (UV),

Figure 3.2: 3D printed tensile type I specimen.

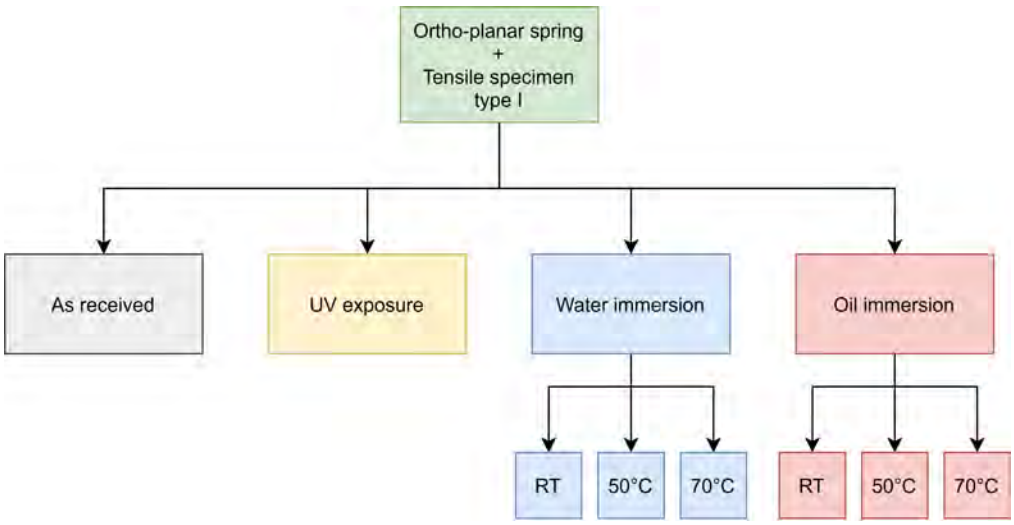

Figure 3.3: Flowchart of the experimental procedure of the work.

water immersion at room temperature (WI-RT), water immersion at 50°C (WI-50), water immersion at 70°C (WI-70), oil immersion at room temperature (OI-RT), oil immersion at 50°C (OI-50) and oil immersion at 70°C (OI-70).

3.1 Material

The material chosen was acrylonitrile buradiene styrene (ABS), due to its good mechanical properties and wide use in engineering applications, as already described in Section 2.3.

The density of the ABS filament used in the printing was 1060kg/m^3, which would technically enable an easier aging in water or oil immersion, as the density of these liquids is lower than the density of the filament. Although the nominal infill percentage of the printing was 100% for both specimens, the TS samples showed lower density than water, indicating that the infill percentage is smaller than 100%. This was verified when the samples were placed in water and tended to stay on the surface. The 3D printed OPS samples seemed to have density close to the filament density, which indicates that the infill was near 100%. The samples had no problem of being immersed in oil, as the oil density is lower than the water density.

As the infill percentage has a direct impact on the mechanical properties of printed materials, it becomes important to know what is the density and infill characteristics of the samples. To calculate an approximation of the density and infill percentage, the height of the samples, their surface area and their weight were used to calculate the volume and density. The calculated density was then compared with the density of ABS filament to find the infill percentage.

The approximate calculated density and infill percentage are shown in Table 3.1. As can be seen, the infill percentage of the samples is indeed far from 100%. The global mean value of the infill percentage was 74.59%. Although this issue was not expected, it did not make the analysis invalid. The only thing to keep in mind is the difference of infill percentage between AR samples and the other conditions, once higher levels of infill indicate improved mechanical properties [44].

Table 3.1: Approximate calculated mean density and infill percentage values of the 3D printed tensile samples.

Condition	Density [kg/m^3]	Variation from AR	Approximate infill percentage [%]
AR	778.55 ± 74.51	-	73.45 ± 7.03%
UV	817.52 ± 46.16	+5.00%	77.12 ± 4.35%
WI-RT	803.81 ± 84.56	+3.24%	75.83 ± 7.98%
WI-50	768.04 ± 107.04	-1.35%	72.46 ± 10.10%
WI-70	770.77 ± 79.64	-1.00%	72.71 ± 7.51%
OI-RT	780.02 ± 56.40	+0.19%	73.59 ± 5.32%
OI-50	776.74 ± 53.01	-0.23%	73.28 ± 5.00%
OI-70	829.62 ± 19.05	+6.56%	78.27 ± 1.80%

To evaluate the approximate density and infill percentage of OPS samples, one can check the section properties of the STL file and get the top surface area. By multiplying it by the thickness of the mechanism, the volume is calculated and then dividing the measured weight by this result, the density is found. Finally, by dividing the approximate density by the density of ABS the infill percentage is estimated. The results are listed in Table 3.2. The global mean value of the infill percentage was 91.31%.

Table 3.2: Approximate calculated mean density and infill percentage values of the 3D printed OPS samples.

Condition	Density [kg/m^3]	Variation from AR	Approximate infill percentage [%]
AR	985.66 ± 17.13	-	92.99 ± 1.62%
UV	995.65 ± 17.71	+1.01%	93.93 ± 1.67%
WI-RT	968.67 ± 65.55	-1.72%	91.38 ± 6.18%
WI-50	951.79 ± 59.05	-3.44%	89.79 ± 5.57%
WI-70	1000.64 ± 55.04	1.52%	94.40 ± 5.19%
OI-RT	965.32 ± 18.61	-2.06%	91.07 ± 1.76%
OI-50	957.67 ± 29.64	-2.84%	90.35 ± 2.80%
OI-70	917.76 ± 24.32	-6.89%	86.58 ± 2.29%

3.2 Printing of specimens and test setup

The specimens were 3D printed in a GTMax3D H5 printer with the settings listed in Table 3.3. As the height of the mechanism was 3.6mm, 12 layers of printing were necessary.

Printing settings	Values
Material	ABS
Layer height	0.3mm
Infill	100%
Temperature	220°C (nozzle) 110°C (heated bed)
Printing speed	60mm/s
Raster angle	45°/-45°

Table 3.3: 3D printing settings used for the fabrication of tensile and OPS samples.

Due to the difference in the real infill percentage of the OPS and TS samples, the mechanical properties of the TS samples were not used to evaluate the analytical and numerical mechanical behavior of the OPS samples, once it would lead to wrong results. In Item 5.2, the alternative used was explained.

The printed ortho-planar spring can be seen in Fig. 3.4, which contains 6 auxiliary holes to fix the mechanism with bolts and screws in the mechanical setup designed for these samples.

Figure 3.4: Printed ortho-planar spring mechanism with 6 auxiliary holes.

Before the aging, all samples were measured, weighted and cataloged. A numbered seal was placed in each one for identification. To properly perform the aging, it was necessary to create a special setup for the hygrothermal and UV agings, once it is required that the specimens are separated from each other to avoid any kind of interference during the process. The hygrothermal aging setup can be seen in Fig. 3.5 and the UV aging setup is shown in Fig. 3.6 for the ortho-planar spring specimens. The hygrothermal setup was made with auxiliary ABS parts printed in black color, which formed a circular shelf structure to hold the mechanisms with a distance of approximately 10mm between the samples. In the UV setup, bolts and screws were preferred, once it creates a more stable structure.

Figure 3.5: Setup for the water and oil immersion agings of the ortho-planar spring with auxiliary printed parts.

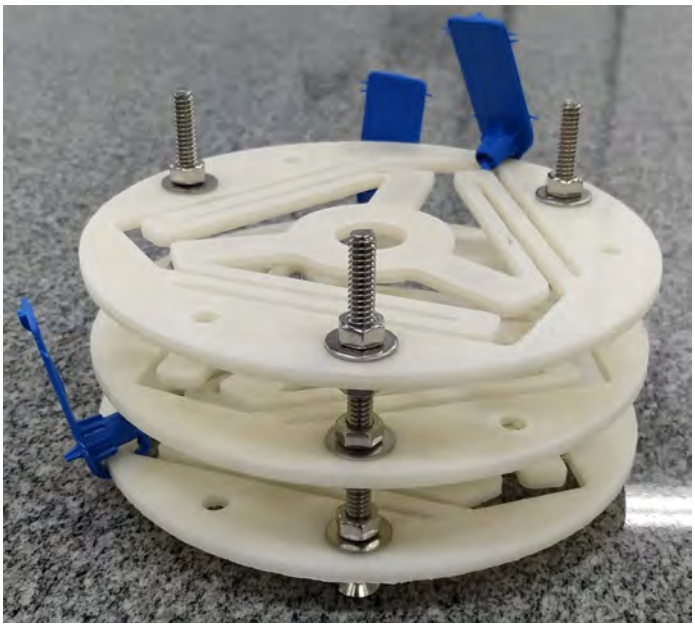

Figure 3.6: Setup for the UV aging of the ortho-planar spring with bolts and screws.

An aging setup was also created for the tensile specimens, as can be seen in Fig. 3.7. This auxiliary structure was used in both UV and hygrothermal agings.

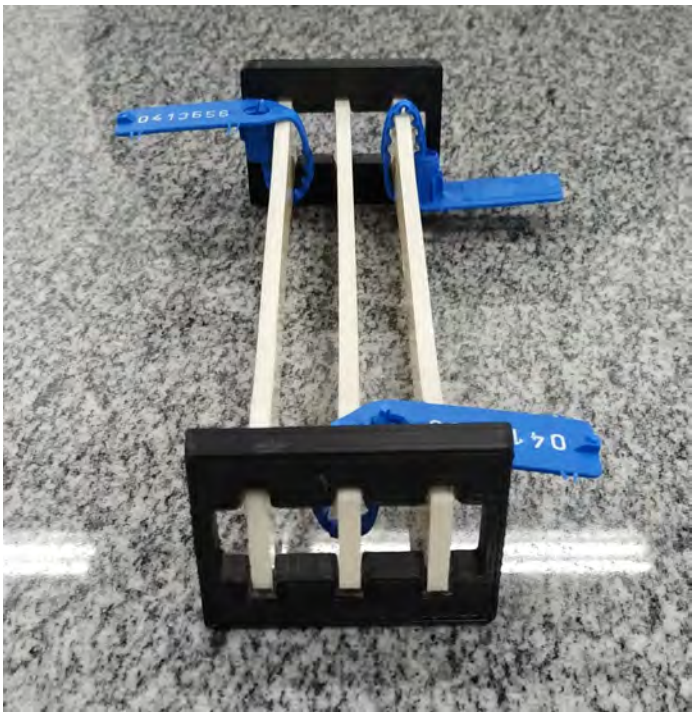

Figure 3.7: Aging setup for the tensile specimens for the UV and hygrothermal agings.

3.3 Aging of specimens

Samples of UV and hygrothermal agings of the tensile and OPS specimens were submitted to these aging conditions for 180 days (6 months) before testing.

In the UV aging, a UV dark chamber was used (Fig. 3.8). The light inside the equipment had wavelength of 264nm and 8W of power. The OPS samples were arranged in the structure shown in Fig. 3.6, but with the screws parallel to the floor of the equipment to prevent that one sample creates a shadow on the surface of another sample. Tensile samples were arranged according to Fig. 3.7. All OPS and tensile samples were monthly rotated by 180 degrees, enabling a homogeneous incidence of radiation on both sides.

As already mentioned, two types of hygrothermal aging were performed. The first one was a water immersion aging, being tap water the liquid used. In the oil immersion aging, the Shell Helix HX7 10W40 API SN semi-synthetic engine lubricating oil was used. The choice of tap water is due to the fact that possible aging situations come from exposure to rain, humidity inside a certain room or partial/complete immersion in water. The choice of the oil makes sense when we think that a possible application for this compliant mechanism is inside a equipment or engine that requires oil to lubricate it.

The laboratory equipment used for the hygrothermal agings was a

Figure 3.8: UV dark chamber used in the ultraviolet radiation aging.

Novatecnica NT 265 water bath (Fig. 3.9). All samples from a certain condition were properly arranged in their setup structures (as shown in Figs. 3.5 and 3.7) and placed inside a glass recipient containing tap water or oil. In the case of the room temperature aged samples, their recipients were stored inside a drawer to prevent drastic temperature changes and incidence of light. The room temperature was measured by a thermocouple and was $23 \pm 0.50°C$.

Figure 3.9: Water bath equipment used in the water and oil immersion agings.

3.4 Mechanical testing

The mechanical tests of both specimens were carried out in an AME-2kN universal testing machine (Fig. 3.10). The specifications of the tests on each specimen are described in Table 3.4.

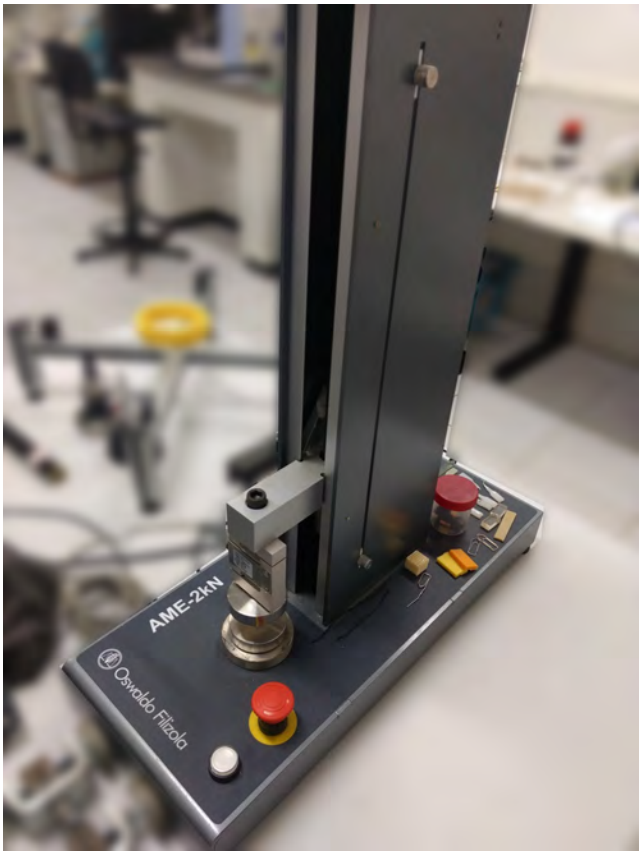

Figure 3.10: AME-2kN universal testing machine used in the mechanical tests of OPS and tensile samples.

Table 3.4: Specifications of the mechanical tests of the tensile and OPS samples.

Specification	Tensile samples	OPS samples
Test type	Tensile	Tensile
Test speed rate	5mm/min	5mm/min
Maximum displacement	Until breakage	20% of flexible member length
Samples per aging condition	3	3
Number of tests	1	5

The mechanical setup of the OPS specimen is shown in Fig. 3.11. It was made with 3D printed ABS parts, bolts and screws. The structure was fixed in an AME-2kN universal testing machine, with maximum load capacity of 2kN. With the structure fixed at the base, a sample was attached to the moving piece of the equipment, enabling the tensile test of an ortho-planar spring. The fixation of the samples was done manually without the use of a torquemeter.

Figure 3.11: Mechanical testing setup of an ortho-planar spring.

The tensile samples were tested using grips to hold both ends of the specimen separated by a distance of 115mm (Fig. 3.12), which is the distance proposed by ASTM D638 [89].

The straight line between 1% and 2% of strain was used to calculate the Young's modulus of tensile samples. In this calculus, instead of using the gage length distance of 50mm, the distance between grips was used to calculate the strain, once strain gauges were not used in the tensile tests. If the gage length distance was used, the results could be misleading.

Figure 3.12: Tensile sample placed in the AME-2kN universal testing machine for the tensile test.

3.5 Colorimetric test

To properly analyze the color change of samples after aging, colorimetric tests were performed in both specimens with aid of the equipment Delta Vista 450g, Fig. 3.13, from the company Delta Color. On each sample, a total of 10 measurements were made, with the objective to have an average result and minimize any test error. An example of a colorimetric test in an ortho-planar spring is shown in Fig. 3.14.

The settings used in the measurements were: D65 illuminant, observer 10°, optical geometry 45/0° with brightness of 60° and circular measurement area of 4mm of diameter.

The result of the tests that is of interest to this work is the CIE L*a*b* color scale that can be represented by a Cartesian coordinate system, where L* is the one that defines the luminosity between light (negative L*) and dark (positive L*), a* the one associated with the variation of the red (positive a*) and green (negative a*) color and b* associated with the variation between the yellow (positive b*) and blue (negative b*) color [74].

To compare the color of samples from a certain aging condition with AR

Figure 3.13: Colorimetry equipment Delta Vista from the company Delta Color used in the tests.

Figure 3.14: Colorimetric test of an ortho-planar spring.

samples, one can use Eq. (3-1), where ΔE represents difference in color of samples and the other deltas inside the square root represent the differences in luminosity, difference in the red/green axis and difference in the yellow/blue axis of the coordinate system, respectively.

$$\Delta E = \sqrt{(\Delta L^*)^2 + (\Delta a^*)^2 + (\Delta b^*)^2} \tag{3-1}$$

The perception of color change varies from one person to another. Therefore, color intervals of ΔE were created to distinguish color variation as follows [66]:

– $\Delta E < 1$: color change is not noticed by human eyes;

– $1 \leq \Delta E < 3.3$: color change is noticed by trained operators only;

– $\Delta E \geq 3.3$: color change is noticed by anyone.

These intervals were used in the results chapter to analyze color change of tensile and OPS samples. The variations of L^*, a^* and b^* were also analyzed to report if samples were lighter/darker (L^*), redder/greener (a^*) and yellower/bluer (b^*) when compared to AR samples.

3.6 Water analysis

The tap water used in this work was analyzed before and after the aging processes to verify if there was hydrolysis in the ABS during aging. Characteristics such as pH, amount of suspended particles, and color changes are of interest to this work. The tests were performed by a technician in the Chemistry laboratory of PUC-Rio. Four samples of water were collected as follows:

– Laboratory tap water;

– Water from the recipient that was used to age OPS samples at room temperature;

– Water from the recipient that was used to age OPS samples at 50°;

– Water from the recipient that was used to age OPS samples at 70° ;

The calculus of apparent color, pH and conductivity followed the standards NBR 13798-97, ASTM D1293-12 and ASTM D1125-95, respectively.

4
Numerical and analytical analysis

Numerical and analytical analysis investigations were conducted in this work to compare with the experimental results of the OPS samples. The finite element software Abaqus/CAE was used for the finite element analysis (FEA) and the Pseudo-Rigid-Body Model was used in the analytical analysis. In this chapter, the steps required to model the specimen in Abaqus and in the PRBM were described.

4.1
Abaqus/CAE

Abaqus/CAE is a software that uses FEA to solve non-linear problems. In this work, it was used to test the OPS specimen. A python script was written to automate the process of 3D model creation, material choice and configuration of settings. With the script, it was possible to queue the analysis of multiple mechanisms. For more information regarding Abaqus scripting with python, please check the work of Puri [90]. The steps required to run the analysis in Abaqus are illustrated in Fig. 4.1 and explained in the following sequence.

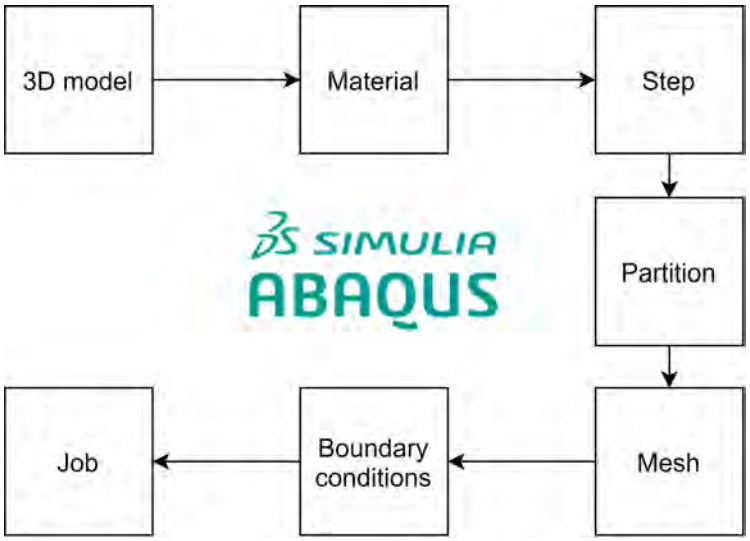

Figure 4.1: Steps required to run the analysis in Abaqus.

1. First, it is necessary to create the 3D model by modeling it inside Abaqus or importing a compatible 3D file. The modeling was done via the python

script, which made this step extremely fast. As the ortho-planar spring has three identical legs, only one of the legs was modeled to decrease analysis time. The final force values results needed to be multiplied by 3 to match the whole mechanism.

2. Then, a material is assigned to the model with the desired specifications. Here, the Young's modulus, density and Poisson's ratio of ABS AR tensile samples were assigned.

3. Now, it is important to define the analysis step, i.e., there are different analysis available in Abaqus. In this work, the Static Analysis step was chosen as the model deals with a static load.

4. The partition is an optional step and depends on the mechanism under analysis. Sometimes the mesh of a part needs some refinement to avoid errors and to improve the analysis of your model. Two partitions were added to the spring at the end of the leg length to refine the mesh, once the mesh tend to curve at that region, forcing the nodes to be extremely close to each other.

5. The next step is to generate the mesh of your model. A C3D8R element with enhanced hourglass control was used for the mesh and with an approximate element size of 0.5mm. The meshed specimen can be seen in Fig. 4.2 (a).

6. A boundary condition (BC) can be configured to the model in the *Load* menu. The ortho-planar spring had one of the leg ends fixed and the other one had a displacement BC assigned. The BCs are illustrated in Fig. 4.2 (b).

7. Finally, it is necessary to create a job to run the analysis. Here, it is possible to change some parameters for faster executions, e.g., one can check the *Use multiple processors* option in the *Parallelization* tab and assign a value compatible to the machine that is going to perform the analysis.

As already mentioned, this whole process was automatized using a python script specifically programmed for this mechanism, which improved the speed of the analysis of a sample, especially modeling time. When doing this configurations by hand (including the modeling), the process usually takes from 10 to 15 minutes. The script does the modeling and configurations in less than 10 seconds, which is a time reduction of almost 98%. The time needed for

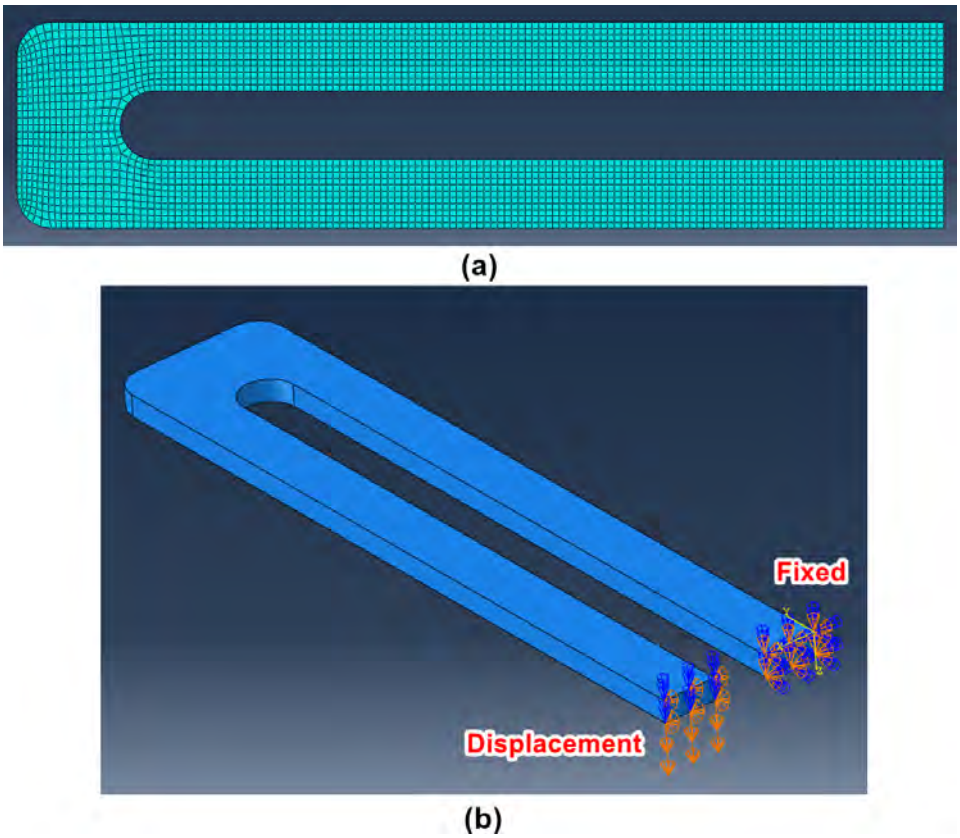

Figure 4.2: (a) Model of the meshed specimen in Abaqus/CAE and (b) its boundary conditions.

the analysis to complete is the same for both processes and it varies depending on the mechanism and mesh settings. The machine used in these analysis had a i7-7700HQ processor.

4.2 Pseudo-Rigid-Body Model

The analytical modeling of the OPS specimen using the PRBM was performed by Parise et al. [11] and will serve as a basis for this section.

The force-displacement behavior of the flexible fixed-guided segments of the OPS (flexible members) can be described by the well-known spring equation in Eq. (4-1), where F is force, δ is the displacement and k is the spring constant.

$$F = k\delta \tag{4-1}$$

As the mechanism analyzed here contains only one flexible member between the base and intermediate platform and one between the platform and intermediate platform, the force applied to these segments are described by Eqs. (4-2) and (4-3), respectively.

$$F_A = k\delta_A \tag{4-2}$$

$$F_B = k\delta_B \tag{4-3}$$

The displacement of the platform can be calculated by

$$\delta_p = \frac{F_A}{k_A} + \frac{F_B}{k_B} \ , \tag{4-4}$$

but $F_A = F_B = F$, which results in

$$\delta_p = \left(\frac{k_A + k_B}{k_A k_B}\right) F \tag{4-5}$$

or

$$F = \left(\frac{k_A k_B}{k_A + k_B}\right) \delta_p \ . \tag{4-6}$$

For all legs, the total spring constant is

$$k_{total} = s\frac{k_A k_B}{k_A + k_B} = s\frac{k}{2} = \frac{3}{2}k \ , \tag{4-7}$$

where s is the number of legs and assuming $k_A = k_B = k$.

For small deflections, the displacement of a flexible member is described by the expression [91]

$$\delta = F\frac{L^3}{12EI} \ . \tag{4-8}$$

By comparing Eqs. (4-1) and (4-8), an expression for the spring constant can be formulated as follows:

$$k = \frac{12EI}{L^3} \ . \tag{4-9}$$

By joining Eqs. (4-1) (4-7) and (4-9), the force-displacement relationship for small deflections of the OPS mechanism can then be written as

$$F = \frac{18EI}{L^3}\delta_p \ . \tag{4-10}$$

For large deflections and considering that the deflection between the base and intermediate platform is the same between the intermediate platform and the platform, the force-displacement relationship can be expressed by

$$F = \frac{4sK_\Theta EI\Theta}{L^2\cos\Theta} = \frac{12K_\Theta EI\Theta}{L^2\cos\Theta} \ , \tag{4-11}$$

where Θ is the pseudo-rigid-body angle of the link and can be expressed by

$$\Theta = \arcsin\frac{\delta_p}{2\gamma L} \ , \tag{4-12}$$

where γ is the characteristic radius factor (usually $\gamma \approx 0.85$) [2] and K_Θ is the stiffness coefficient (usually $K_\Theta \approx 2.65$) [92].

Now, one can use Eq. (4-10) to model an OPS when subjected to small deflections or Eq. (4-11) for large deflections. In this work, the first equation

was adopted as deflections were low compared to the flexible member length. The software MATLAB was used to iterate the calculation of the PRBM force values when varying the displacement.

5
Results and discussion

In this chapter, the results of the mechanical tests of the TS and OPS samples were analyzed in separate sections. In the last section, a comparison between the aging effects in both specimens was made.

Throughout this chapter, the variation of properties will be presented many times. Thus, to improve reading and comprehension, the variations will always be relative to the AR samples unless stated otherwise.

As already discussed in Item 3.1, samples presented different infill percentages, which affect the comparison between aged and AR samples. To overcome that, a correction of the mechanical properties considering the difference of infill was performed by linear interpolation, because properties tend to increase linearly after 70% infill [44]. If the samples of a certain condition, for example, have infill higher than AR samples, then the original properties of these samples would be originally higher. The correction procedure, explained in the diagram of Fig. 5.1 for an arbitrary aging condition and property, consisted of calculating an approximation of the original properties of the samples before aging and using this value as the comparison base to check the true variation of these properties. For a reliable execution of the statistical tests, the materials used for each sample must be the same, i.e., they should have the same infill percentage. Once that is not the case here, the value of the original properties of the samples will be assumed to be equal to the properties of AR samples and the variation calculated considering the actual properties will be applied. Figure 5.1 shows an example of the procedure used. Arbitrary values were used, just to serve as an example. The property of AR samples was considered to be 500 MPa. A value of 400 MPa was determined when the aged sample was tested. The aged sample had, however, a higher infill. So, the actual value of the "as received" sample before aging would be 525 MPa. Therefore, a decrease of 23.8% is to be expected, not just 20%. The corrected property value can, then, be safely used in the statistical tests. It is important to say that this correction procedure assumes that samples with different infills will present equal variation of properties when submitted to an aging condition. Therefore, this procedure aims to get an approximation of the real variations, because infill percentages may impact how aging affects

the samples.

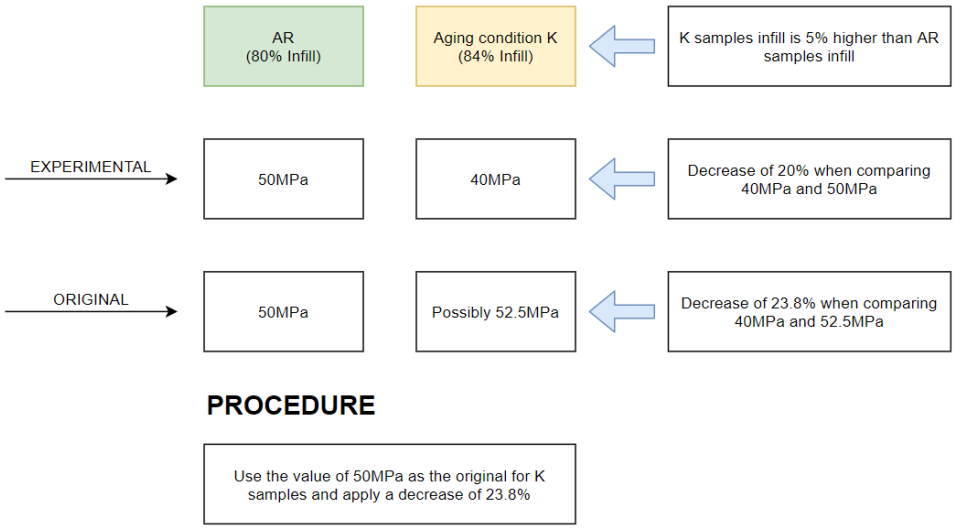

Figure 5.1: Diagram of the correction procedure of the mechanical properties of samples considering the difference of infill percentage.

To check if the variations of the mechanical properties are really a result of the aging and if the means are statistically different from each other, Student's t-tests were performed for both specimens. The mean values of the properties between a certain condition and AR samples were compared. The t-test for equal sample sizes was chosen for this statistical analysis. The null hypothesis assumes that the means of two samples are statistically equal. As the sample size (n=3) is small, a level of significance of 10% was adopted, i.e., if the p-value is smaller or equal to 0.9, the null hypothesis is accepted. If greater than 0.9, it is rejected and the alternate hypothesis is accepted, indicating that the means are statistically different from each other.

5.1 Tensile specimens

In totality, 24 samples of the tensile test type I specimen were subjected to mechanical tensile tests. In Table 5.1, the mechanical properties of the samples of each condition are shown, namely Young's modulus, ultimate strength, elongation at break and toughness. In Table 5.2, the p-value of the Student's t-test of the tensile samples of each condition for all properties is listed. The plot of one tensile sample of each condition is shown in Fig. 5.2. As the failure of all samples was brittle, only the toughness property was calculated, because it would not be possible to distinguish the elastic zone from the plastic zone. The plots of the tensile tests of all samples can be found in Appendix C (page 94).

A comparison of the mechanical properties of the tensile samples with other works in the literature was made at the end of this section, but it can be said that values were considerable different, because the infill percentage was far from 100%. The p-values before the correction procedure show that only the elongation at break was affected in UV samples. In WI samples, only the Young's modulus of WI-70 samples has significantly changed. In OI samples, the Young's modulus of OI-RT and OI-50 samples has significantly changed. It will be shown after the correction procedure that some of these conclusions will no longer be the same, because the difference of infill percentages was considered.

Table 5.1: Mean values and standard deviation of the mechanical properties of the tensile test type I samples of each condition.

Condition	Young's modulus [MPa]	Ultimate strength [MPa]	Elongation at break [%]	Toughness [MJ/m^3]
AR	640.4 ± 83.4	17.5 ± 2.2	4.1 ± 0.1	0.41 ± 0.07
UV	574.9 ± 24.7	17.6 ± 2.2	3.4 ± 0.2	0.33 ± 0.06
WI-RT	636.7 ± 110.2	19.1 ± 3.8	4.0 ± 0.6	0.41 ± 0.09
WI-50	550.9 ± 79.9	16.9 ± 5.1	4.1 ± 0.4	0.40 ± 0.15
WI-70	520.6 ± 50.5	16.5 ± 4.3	3.7 ± 0.5	0.34 ± 0.13
OI-RT	537.9 ± 63.8	16.2 ± 3.6	4.2 ± 0.5	0.41 ± 0.13
OI-50	518.7 ± 41.5	16.7 ± 3.5	4.4 ± 0.4	0.45 ± 0.10
OI-70	574.8 ± 5.4	19.5 ± 0.3	4.8 ± 0.2	0.56 ± 0.04

Table 5.2: The p-value of the Student's t-test of mechanical properties of the tensile samples of each condition.

Condition	Young's modulus	Ultimate strength	Elongation at break	Toughness
AR	-	-	-	-
UV	0.8689	0.5397	0.9954	0.8948
WI-RT	0.5176	0.7188	0.5872	0.5241
WI-50	0.8746	0.5653	0.5068	0.5378
WI-70	0.9498	0.6306	0.7835	0.7448
OI-RT	0.9169	0.6831	0.6784	0.5162
OI-50	0.9568	0.6116	0.9037	0.7082
OI-70	0.8772	0.9089	0.9966	0.9872

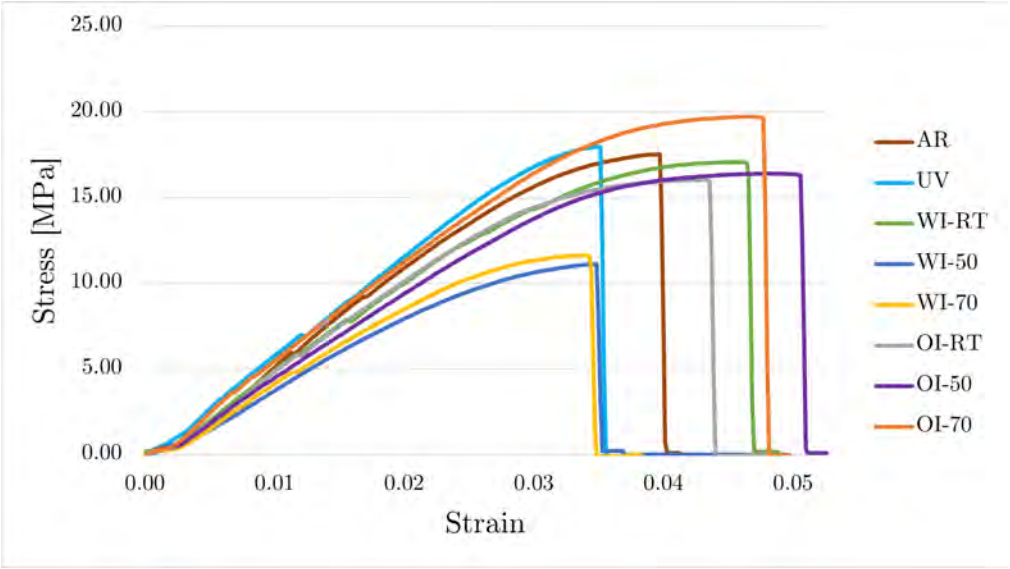

Figure 5.2: Tensile tests of one tensile sample of each condition.

The correction procedure of the mechanical properties of tensile samples was performed and the new p-value of the Student's t-test of each condition for all properties is listed in Table 5.4. In Table 5.3, the variations of the corrected mechanical properties are presented. The discussions of results will now be related to the corrected values, unless stated otherwise.

Table 5.3: Mean variations of the corrected mechanical properties of the tensile test type I samples of each condition.

Condition	Young's modulus	Ultimate strength	Elongation at break	Toughness
AR	-	-	-	-
UV	-14.5%	-3.7%	-19.3%	-22.9%
WI-RT	-3.7%	+5.8%	-5.1%	-2.1%
WI-50	-12.8%	-1.9%	+1.5%	-1.1%
WI-70	-17.9%	-4.7%	-6.1%	-14.4%
OI-RT	-16.2%	-7.4%	+3.3%	+0.7%
OI-50	+4.6%	-3.9%	+10.1%	+10.5%
OI-70	-15.8%	+5.0%	+10.6%	+30.1%

It is important to mention that due to an issue in the test equipment, the tensile tests of two samples of WI-RT were interrupted before the sample could break. Therefore, the variation in the ultimate strength could be higher. Therefore, the maximum achieved stress value will be used as the ultimate strength.

Table 5.4: The p-value of the Student's t-test of the corrected mechanical properties of the tensile samples of each condition.

Condition	Young's modulus	Ultimate strength	Elongation at break	Toughness
AR	-	-	-	-
UV	0.9315	0.6335	0.9982	0.9291
WI-RT	0.6117	0.6475	0.7124	0.5512
WI-50	0.8553	0.5384	0.5828	0.5167
WI-70	0.9438	0.6087	0.7519	0.7319
OI-RT	0.9186	0.6872	0.6695	0.5128
OI-50	0.6943	0.6056	0.9078	0.7124
OI-70	0.9478	0.7325	0.9835	0.9740

Specimens exposed to hygrothermal aging were already expected to present inferior mechanical properties. In WI samples, the decrease in Young's modulus was only significant at 70°C with a variation of -17.9%, because higher temperatures can cause faster plasticization, more aggressive hydrolysis or swelling-induced microcracking [72]. Although the results may show a downtrend in properties, the only considerable statistical variation in WI samples in all properties was in the Young's modulus of WI-70 samples.

The decrease of properties in oil aged polymers was investigated by Amaral [74]. Both of his samples (PA 12 and HDPE) presented a decrease in the Young's modulus. On the other hand, HDPE samples showed improved ultimate strength, while PA 12 samples presented a decrease. In this work, OI samples had reduced values for Young's modulus at room temperature and at 70°C.

Since the Young's modulus of WI-RT, WI-50 and OI-50 samples and ultimate strength of all samples were considered statistically equal to the AR samples properties, it can be said that the aging for these conditions was not able to promote a relevant change of the tensile mechanical properties.

In respect to toughness and elongation at break, UV aging caused the most severe, and statistically significant, reduction of properties (Tables 5.4 and 5.3). For WI samples, both elongation at break and toughness were statistically equal to AR samples, although toughness presented a trend of decrease. In OI-70 samples, the elongation at break increased 10.6%. The toughness presented the same pattern, increasing in OI samples. This increase may be due to an improvement in material flexibility, as already seen by Pereira et al. [75] in oil aged HDPE. The toughness of OI-RT and OI-50 samples

and the elongation at break of OI-RT samples were statistically equal to AR samples.

The weight of the samples was measured before and after the aging processes and it is listed in Table 5.5. The weight variation of UV samples was higher than all WI samples. All aging conditions caused the samples to absorb a significant amount of liquid. The variations of OI samples were higher than WI samples, indicating that ABS tends to absorb more oil than water. These high variations can be explained by the infill percentage values of the tensile samples shown in Item 3.1 (page 42). The lower the infill, the higher is the number of voids inside the structure, which will naturally allow more paths for the liquid to enter and stay.

Table 5.5: Mean weight of the tensile test type I samples of each condition before and after the aging processes. The variations were measured by using the weights of each condition and not the weight of AR samples.

Condition	Weight [g]	Weight after [g]	Variation
AR	6.4 ± 0.6	-	-
UV	6.7 ± 0.5	7.7 ± 0.5	+20.1%
WI-RT	6.6 ± 0.6	7.2 ± 0.4	+12.4%
WI-50	6.3 ± 0.9	7.5 ± 0.7	+16.0%
WI-70	6.3 ± 0.7	7.4 ± 0.7	+15.4%
OI-RT	6.4 ± 0.7	7.6 ± 0.4	+18.7%
OI-50	6.5 ± 0.6	7.8 ± 0.4	+20.6%
OI-70	6.8 ± 0.1	8.1 ± 0.1	+25.4%

Works in the literature often report an increase of the Young's modulus after UV exposure [6, 84]. Here, UV samples had a decrease of 14.5%. This can be explained by the considerable amount of moisture absorbed inside the UV dark chamber, causing plasticization and eventually decreasing molecular interactions [93]. If samples had a higher infill, the moisture absorption would be much lower and then the true impact of UV acting in isolation would be better analyzed. Kakanuru and Pochiraju [86] reported a maximum moisture gain of only 0.67% in their 3D printed ABS samples with 100% infill submitted to distilled water at 50°C. Therefore, the weight variations were indeed associated with the infill percentage.

When compared to other works in the literature (Table 5.6), one can see that the Young's modulus and ultimate strength of the AR samples of this work is significantly smaller, which can be explained by the use of a different

fabrication process or 3D printers. The reduced infill percentage issue of the tensile samples also made them less stiff than expected.

Table 5.6: Comparison of the mechanical properties of the AR tensile test type I samples with works in the literature.

Reference (Fabrication process)	Young's Modulus [MPa]	Ultimate strength [MPa]	Elongation at break [%]
This work (3D printed)	640.40 ± 83.41	17.46 ± 2.21	4.04 ± 0.12
Fiorio et al. [84] (Injection molded)	1950 ± 70	32.2 ± 0.2	-
Kakanuru and Pochiraju [86] (3D printed)	2800	38.64	3.41
Popescu et al. [87] (3D printed)	1833.33	21.66	1.50

The UV, WI-70 and OI-70 samples presented the most noticeable change in color. Despite having absorbed the most quantity of oil, OI-70 samples were lighter than WI-70 ones, indicating the possibility of a more severe chemical degradation of WI-70 samples. The color of WI-70 and OI-70 samples changed from white to a brown scale, while UV samples tended to a light yellow tone. The samples of all conditions are presented in Fig. 5.3.

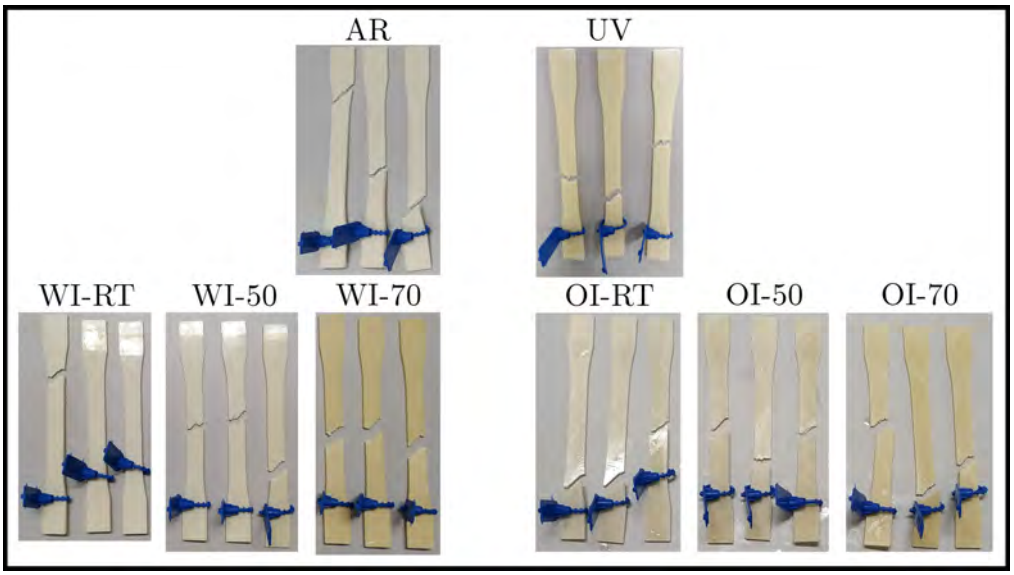

Figure 5.3: Tensile samples of each condition after aging and mechanical tests.

The colorimetric tests were performed for tensile samples and the values of ΔE, ΔL^*, Δa^* and Δb^* of each condition are shown in Table 5.7.

Table 5.7: The values of ΔE, ΔL^*, Δa^* and Δb^* measured by the colorimetric tests for each condition of the tensile samples.

Condition	ΔE	ΔL^*	Δa^*	Δb^*
AR	-	-	-	-
UV	11.2 ± 0.9	-1.6 ± 1.0	-0.4 ± 0.2	11.0 ± 0.9
WI-RT	1.7 ± 1.2	-0.1 ± 2.0	0.2 ± 0.3	-0.6 ± 1.2
WI-50	1.4 ± 0.8	1.1 ± 1.2	-0.2 ± 0.1	0.0 ± 0.8
WI-70	9.4 ± 0.8	4.1 ± 1.5	2.3 ± 0.2	8.0 ± 0.7
OI-RT	2.5 ± 0.3	-1.8 ± 0.7	0.2 ± 0.1	-1.6 ± 0.4
OI-50	4.2 ± 2.0	-4.1 ± 2.1	0.2 ± 0.1	-0.8 ± 0.7
OI-70	8.4 ± 1.4	-6.1 ± 2.5	0.1 ± 0.3	5.5 ± 1.0

The color tests confirm that UV, WI-70 and OI-70 samples present the highest color difference (ΔE) of all conditions. In OI samples, ΔE gets higher as the temperature is increased. On the other hand, WI-RT and WI-50 samples had modest modifications, being statistically equal.

In Table 5.8, the interpretation of the colorimetric test results was made for each condition. The UV, WI-70, OI-50 and OI-70 samples were visible by anyone, which makes sense when one look back at Fig. 5.3 and see that those groups stand out more. In general, tensile samples were lighter and redder than AR samples.

Table 5.8: Interpretation of the values of ΔE, ΔL^*, Δa^* and Δb^* measured by the colorimetric tests for each condition of the tensile samples.

Condition	ΔE	ΔL^*	Δa^*	Δb^*
AR	-	-	-	-
UV	Visible by anyone	Lighter	Greener	Yellower
WI-RT	Visible by operators	Lighter	Redder	Bluer
WI-50	Visible by operators	Darker	Greener	No change
WI-70	Visible by anyone	Darker	Redder	Yellower
OI-RT	Visible by operators	Lighter	Redder	Bluer
OI-50	Visible by anyone	Lighter	Redder	Bluer
OI-70	Visible by anyone	Lighter	Redder	Yellower

5.2 Ortho-planar spring specimens

In totality, 24 samples of the ortho-planar spring specimen were submitted to mechanical tests. In Table 5.9, the mechanical properties mean values of each condition are shown, namely spring constant, force at 20% of the flexible member length (FML) and Young's modulus of flexible member (FM). In Table 5.10, the p-value of the Student's t-test of OPS samples of each condition for all properties is listed. The plot of the mechanical tests of one OPS sample of each condition compared with the Abaqus/CAE and PRBM results is shown in Fig. 5.4. The plots of the tests of all samples can be found in Appendix D (page 98). Each mechanism was tested five times and in each test a displacement of 20% FML (10.30mm) was applied.

The p-values before the correction procedure only present two statistically significant results, namely, spring constant and force at 20% FML of WI-RT samples. It will be shown later that after the correction, only two additional results became statistically significant.

The correction procedure of mechanical properties of OPS samples was performed and the new p-value of the Student's t-test of each condition for all properties is listed in Table 5.12. In Table 5.11, the variations of the corrected mechanical properties are presented. The discussions of results will now be related to the corrected values, unless stated otherwise.

As can be seen in Fig. 5.4, the mechanical behavior predicted by Abaqus and PRBM is different from the experimental results. One possible cause may be related to the universal testing machine used, because it cannot be considered rigid and suffer elastic displacements during a test.

Table 5.9: Mean values and standard deviation of the mechanical properties of the ortho-planar spring samples of each condition.

Condition	Spring constant [N.m]	Force at 20% FML [N]	Young's modulus of FM [MPa]
AR	1439.9 ± 115.3	23.4 ± 3.3	1647.4 ± 72.6
UV	1335.7 ± 36.2	21.4 ± 1.0	1617.1 ± 279.8
WI-RT	1562.5 ± 63.9	27.5 ± 1.9	1881.8 ± 273.6
WI-50	1348.1 ± 105.1	18.9 ± 5.3	1417.3 ± 345.1
WI-70	1507.8 ± 75.4	27.0 ± 4.7	1710.6 ± 295.7
OI-RT	1408.1 ± 99.2	25.4 ± 7.8	1706.4 ± 283.5
OI-50	1529.3 ± 141.6	26.2 ± 3.1	1572.5 ± 347.1
OI-70	1513.2 ± 180.2	26.0 ± 7.1	1556.2 ± 195.8

Table 5.10: The p-value of the Student's t-test of mechanical properties of the OPS samples of each condition.

Condition	Spring constant	Force at 20% FML	Young's modulus of FM
AR	-	-	-
UV	0.8953	0.8127	0.5676
WI-RT	0.9087	0.9351	0.8875
WI-50	0.8173	0.8606	0.8392
WI-70	0.7794	0.8328	0.6313
OI-RT	0.6322	0.6513	0.6277
OI-50	0.7779	0.8300	0.6334
OI-70	0.7076	0.7019	0.7542

This phenomenon is more pronounced in the initial test region, close to the resolution limit of the equipment, between 0 to 20N. As the tests of the mechanisms stayed close to this range, the results were affected by the testing machine and the expected linear behavior from the beginning of the test was not present. Once it is difficult to compare the experimental curves with the numerical ones, only the experimental values will be compared between each other. As already said, the complete tensile test force-displacement curves of all samples are shown in Appendix D (page 98).

The spring constant was calculated by the slope of the straight line between 3% and 20% FML, because in this region that is when the spring starts its expected linear behavior. The results of Table 5.9 regarding the spring

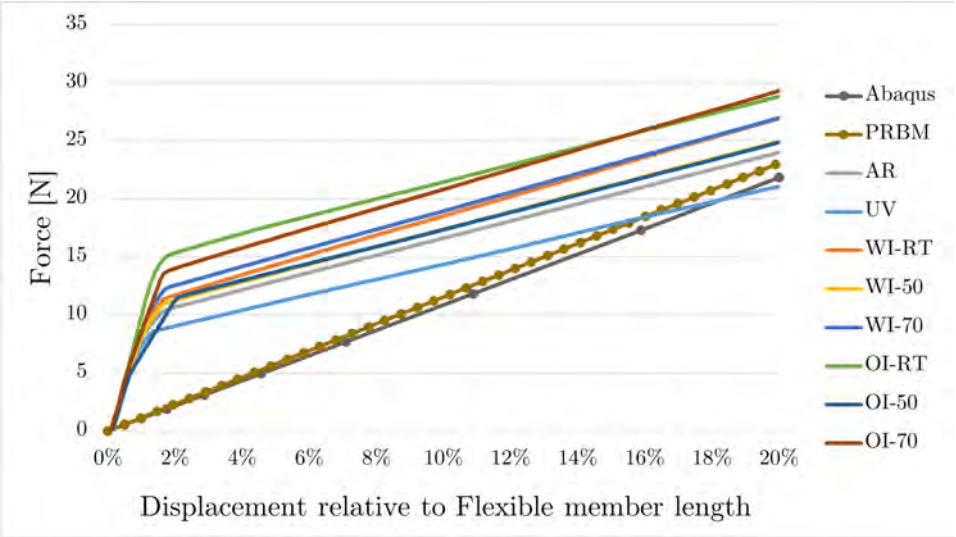

Figure 5.4: Mechanical tests of one OPS sample of each condition compared to the Abaqus/CAE and PRBM results.

Table 5.11: Variations of the corrected mechanical properties of the OPS samples of each condition.

Condition	Spring constant	Force at 20% FML	Young's modulus of FM
AR	-	-	-
UV	-8.2%	-9.4%	-2.8%
WI-RT	+20.2%	+32.3%	+19.6%
WI-50	-12.2%	-30.2%	-23.3%
WI-70	+6.4%	+36.0%	+14.8%
OI-RT	-3.2%	-2.4%	+3.4%
OI-50	+9.5%	+3.9%	-7.1%
OI-70	+3.2%	+3.5%	+3.3%

constant and force at 20% FML would be more relevant if the mechanical tests did not present the mentioned issue and the geometric variation of samples was not significant.

An alternative to check the effect of aging in OPS samples is to check if the Young's modulus of the flexible members has changed. This can be done by taking Eq. (4-10) and using the force at 20% FML in the calculation along with the moment of inertia, which takes the mean width of all FMs and the height of the mechanism.

By looking at the p-values in Table 5.12, only the spring constant of UV samples and properties of WI-RT samples are statistically different from the

Table 5.12: The p-value of the Student's t-test of the corrected mechanical properties of the OPS samples of each condition.

Condition	Spring constant	Force at 20% FML	Young's modulus of FM
AR	-	-	-
UV	0.9167	0.8350	0.6038
WI-RT	0.9394	0.9489	0.9086
WI-50	0.6717	0.8211	0.7792
WI-70	0.7013	0.8096	0.5806
OI-RT	0.5090	0.6843	0.6945
OI-50	0.8603	0.8770	0.5513
OI-70	0.8863	0.8002	0.5693

AR samples. Therefore, it cannot be said that the aging significantly affected the mechanical behavior of the mechanism. This is an interesting result that means that the elastic capabilities of ortho-planar springs stay somewhat intact after 6 months of harsh aging conditions of water and oil immersion and UV radiation.

The weight of the samples was measured before and after the aging processes and it is listed in Table 5.13. WI and OI samples absorbed similar quantities of liquid. The UV samples had a more modest weight variation, that was assigned to moisture absorption inside the UV dark chamber.

Table 5.13: Mean weight of the OPS samples of each condition before and after the aging processes. The variations were measured by using the weights of each condition and not the weight of AR samples.

Condition	Weight [g]	Weight after [g]	Variation
AR	24.6 ± 0.7	-	-
UV	24.3 ± 0.4	24.4 ± 0.4	+0.5%
WI-RT	24.8 ± 0.2	25.6 ± 0.3	+3.3%
WI-50	23.4 ± 1.3	24.5 ± 1.1	+4.8%
WI-70	25.5 ± 0.4	26.7 ± 0.8	+4.8%
OI-RT	24.4 ± 1.2	25.3 ± 1.2	+3.5%
OI-50	25.3 ± 0.2	26.4 ± 0.1	+4.3%
OI-70	24.4 ± 1.4	25.5 ± 1.4	+4.6%

The UV, WI-70 and OI-70 samples presented the most noticeable change

in color. Despite having absorbed the most quantity of oil, OI-70 samples were significantly lighter than WI-70 ones, indicating a possible chemical degradation process of WI-70 samples. The color of WI-70 and OI-70 samples changed from white to a brown scale, while UV samples tended to a light yellow tone. The samples of all conditions are shown in Fig. 5.5.

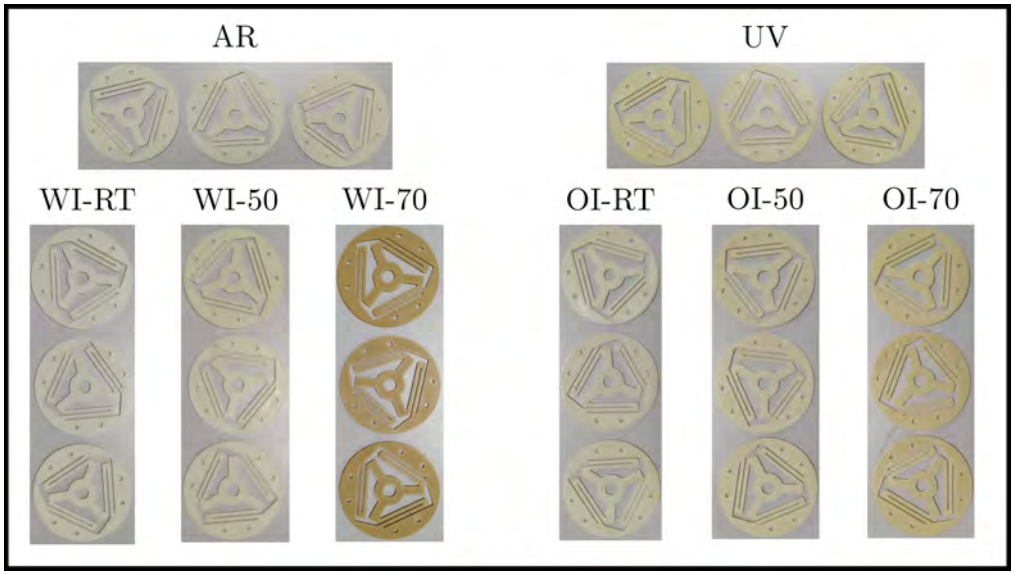

Figure 5.5: OPS samples of each condition after aging and mechanical tests.

The colorimetric tests were performed for tensile samples and the values of ΔE, ΔL^*, Δa^* and Δb^* of each condition are shown in Table 5.14.

Table 5.14: The values of ΔE, ΔL^*, Δa^* and Δb^* measured by the colorimetric tests for each condition of the OPS samples.

Condition	ΔE	ΔL^*	Δa^*	Δb^*
AR	-	-	-	-
UV	10.1 ± 0.9	1.3 ± 2.0	-0.7 ± 0.1	9.8 ± 0.8
WI-RT	6.8 ± 0.5	6.7 ± 0.6	-0.1 ± 0.1	-0.7 ± 1.2
WI-50	6.8 ± 0.5	6.5 ± 0.5	-0.5 ± 0.1	2.1 ± 0.2
WI-70	18.1 ± 0.7	-4.7 ± 2.7	5.0 ± 0.2	16.6 ± 0.2
OI-RT	2.7 ± 0.6	2.5 ± 0.5	-0.4 ± 0.2	-0.7 ± 0.6
OI-50	3.0 ± 1.4	0.7 ± 2.4	-0.5 ± 0.1	2.2 ± 1.2
OI-70	7.8 ± 1.2	-1.2 ± 3.3	-0.3 ± 0.2	7.2 ± 0.8

The color tests confirm that UV, WI-70 and OI-70 samples present the highest color difference (ΔE) of all conditions. Although significant, the changes of room temperature and 50°C in the immersed samples did not seem like to be affected by temperature and more due to the liquid that they are

in contact with. Samples immersed and at 70°C presented notorious color differences in both liquids, which indicates the impact of temperature.

In Table 5.15, the interpretation of the colorimetric test results was made for each condition. Only OI-RT and OI-50 samples were visible by operators and the rest were visible by anyone. In general, OPS samples were darker, greener and yellower than AR samples.

Table 5.15: Interpretation of the values of ΔE, ΔL^*, Δa^* and Δb^* measured by the colorimetric tests for each condition of the OPS samples.

Condition	ΔE	ΔL^*	Δa^*	Δb^*
AR	-	-	-	-
UV	Visible by anyone	Darker	Greener	Yellower
WI-RT	Visible by anyone	Darker	Greener	Bluer
WI-50	Visible by anyone	Darker	Greener	Yellower
WI-70	Visible by anyone	Lighter	Redder	Yellower
OI-RT	Visible by operators	Darker	Greener	Bluer
OI-50	Visible by operators	Darker	Greener	Yellower
OI-70	Visible by anyone	Lighter	Greener	Yellower

5.3 Water analysis

The four samples of water were analyzed and the properties are listed in Table 5.16.

Table 5.16: Properties of the four water samples collected after aging.

Property	AR	RT	50°	70°
Apparent color [HU]	1.4	3.4	5.5	7.3
pH at 25°	6.69	7.09	7.36	7.68
Conductivity at 25° [10^{-6}mhos.cm^{-1}]	132.5	144.5	172.1	218.6
Total dissolved solids [mg.L^{-1}]	94.3	101.9	119.3	148.8

It can be seen that all properties increase after aging and they keep increasing with the temperature. It is important to evaluate those changes, because the liquid is changed and may interfere in other parts of the machine

or mechanism that the CM is present. If the liquid is constantly renewed, this issue is less significant.

It is interesting to analyze the total dissolved solids, because it increases due to the deterioration of samples, which is provoked by hydrolysis.

5.4 Analysis and comparison of results

The objective of this section is to compare the mechanical properties variation of the tensile samples with the OPS samples and to determine if the changes were similar or not and, most importantly, to check how aging processes affect ortho-planar springs and to serve as a base study for other compliant mechanisms.

As a start, the largest difference between the two specimens is the amount of liquid absorbed. Tensile samples showed a variation between 12.4% and 25.4%, while OPS showed smaller variations, between 0.5% and 4.8%. An explanation to this behavior is the difference between infill percentage of the two specimens, which were 74.59% (tensile samples) and 91.31% (OPS samples). A smaller infill percentage is directly proportional to the amount of void inside a sample, which can contribute to a higher degree of fluid absorption. Higher infill will naturally present fewer paths and voids for moisture and liquids to stay.

Now, looking at the mechanical properties, it makes sense to compare the Young's modulus of both specimens. The normalized corrected values of the Young's modulus related to the average of AR samples are presented in Fig. 5.6 (tensile samples) and Fig. 5.7 (OPS samples). All the high deviations shown in the graphs are explained by the effect of aging in samples, submitting them to different levels of degradation, but also by the geometric variation of samples (mainly in the infill percentage), as can be seen in the non-aged AR tensile samples values that could have presented shorter deviations if samples were more similar.

The colorimetric tests performed in both specimens presented similar results and are compared in Table 5.17.

One can see that, in general, the behavior of color change was similar for both specimens, because the ΔE value for UV, WI-RT and OI-70 samples were the biggest in both cases. OPS samples were, in general, darker, greener and yellower after aging, while tensile samples were, in general, lighter and redder after aging. It may be possible that the infill percentage difference was the responsible for this behavior, because all other printing parameters were the same for both specimens.

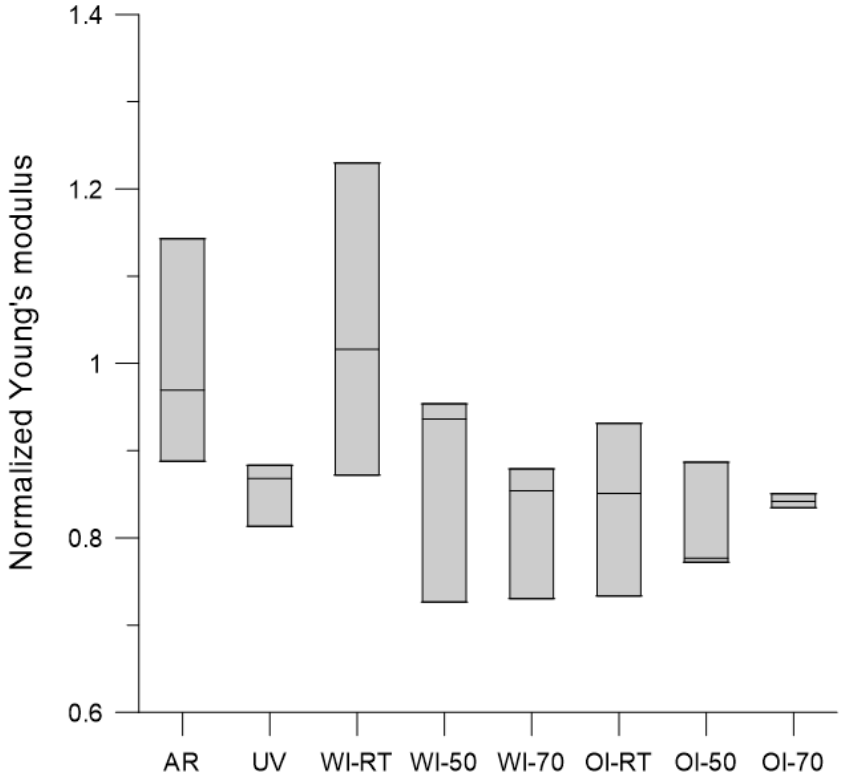

Figure 5.6: Box plot of the normalized Young's modulus of the tensile samples of each condition.

Table 5.17: The values of ΔE measured by the colorimetric tests for each condition of the tensile and OPS samples.

Condition	Tensile samples	OPS samples
AR	-	-
UV	11.2 ± 0.9	10.1 ± 0.1
WI-RT	1.7 ± 1.2	6.8 ± 0.5
WI-50	1.4 ± 0.8	6.8 ± 0.5
WI-70	9.4 ± 0.8	18.1 ± 0.7
OI-RT	2.5 ± 0.3	2.7 ± 0.6
OI-50	4.2 ± 2.0	3.0 ± 1.4
OI-70	8.4 ± 1.4	7.8 ± 1.2

The increase in color difference with the increase of temperature was already seen in other works. Pereira et al. [94] investigated how temperature, aging time and oil type affected the color difference in aged samples. They noticed that the increase in the ΔE was more significant when comparing 50°C and 70°C aged samples, which is a result also seen in this work. In the work of Pereira et al. [94], when temperature increased from 70°C to 90°C, the

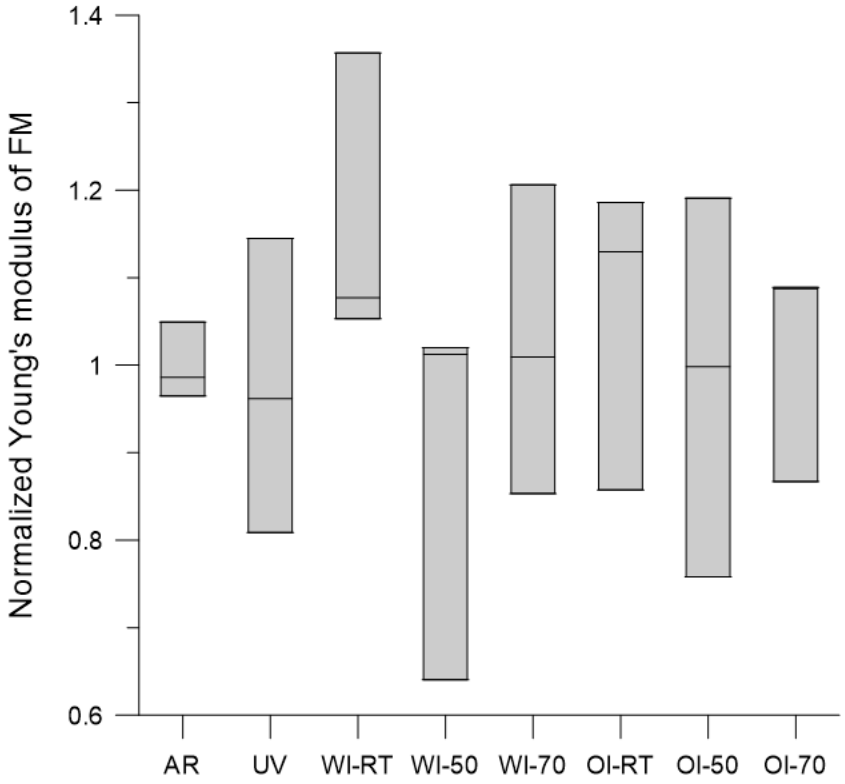

Figure 5.7: Box plot of the normalized Young's modulus of the flexible member of the OPS samples of each condition.

variation was low, which indicated the reach of a color saturation level of the samples. They concluded saying that the most significant variable is the aging temperature. The aging time is also relevant, but not at the same significance level of the temperature. The type of oil used also affected the color, but the variation profile was similar for all oil brands.

WI samples presented a considerable difference in ΔE when comparing both type of specimens. Although a similar pattern can be noticed, this difference may be related to the difference in infill percentage, because the material, exposure time and liquid used were the same.

6
Conclusions

In this work, non-aged and aged samples were submitted to mechanical tests to investigate how aging processes affect the mechanical behavior and elastic capabilities of compliant mechanisms. As polymers often degrade and present decreased mechanical properties after being submitted to aging, it was expected that the mechanisms would also present relevant changes on their compliant behavior after aging. However, other than a possible chemical degradation evidenced by the change in material color, it was not possible to affirm that the aging was indeed responsible for the decrease or increase in the reported mechanical properties.

It is also important to consider the non-expected issues with the samples. Tensile samples presented a global mean of infill percentage of 74.59%, which is far from the designed and expected 100%. Nevertheless, it was possible to analyze the data and compare the variation of mechanical properties for each aging condition. In the case of OPS samples, the infill percentage and geometric dimensions were close to the expected. The standard deviations of the mechanical properties of the aged samples indicate that the aging indeed affected the samples, but not enough to confirm the effect of aging in the mechanical capabilities of OPS samples.

Concerning tensile samples, it can be highlighted important decreases in the Young's modulus in WI-70 (-17.9%), OI-RT (-16.2%) and OI-70 (-15.8%) samples. UV samples also showed a decrease (-14.5%) caused by UV radiation and also by the absorption of moisture inside the UV dark chamber. If the infill was higher, moisture absorption percentage would not be that high. The elongation at break of UV samples and OI samples were also affected, presenting a decrease in UV samples and an increase in OI samples.

The colorimetric tests also showed important color changes. UV, WI-70 and OI-70 samples were the most affected. UV samples were already expected to present this alterations, once it is vastly reported in the literature that ultraviolet radiation causes yellowing of polymers. WI and OI samples presented higher differences with the increase of temperature, especially when going from 50°C to 70°C. A result of the literature [94] confirmed that this behavior is known and the color of samples reach a saturation level at a

temperature higher than 70°C.

The water analysis tests showed an interesting result that all measured water properties increased with aging and continued increasing with higher values of temperature. This is important to know, once the application may be affected by a change in a particular water property.

In short, it can be said that the aging processes affected tensile samples, showing significant variations in the Young's modulus and elongation at break. On the other hand, the same is not true for OPS samples. No statistically significant changes were noticed, which indicates that ortho-planar springs are little or not affected by UV exposure, water or oil immersion aging, under the conditions used in this work. This compliant mechanism, considering the test conditions used in this work, maintained its original mechanical properties and elastic capabilities after six months of aging. Although more testing with the specific materials, environment, and exposure time would be required to verify use in a specific application, the findings of this study suggest that compliant mechanisms show promise for use in applications where aging is a concern, and their life is expected to be within the limits of this aging study.

7
Suggestions for future works

As a first suggestion, it would be interesting to analyze the behavior of the OPS compliant mechanism made of different polymer materials, such as PLA (Polylactic acid) and Nylon (Polyamide) and compare it with the ABS mechanism.

Compliant mechanisms can also be submitted to a variety of other aging conditions, so the aging analysis of this mechanism under different hygrothermal and radiation aging conditions would contribute to a better understanding of its mechanical performance changes.

It would be interesting to subject the mechanism to an aging condition, where the samples would be exposed to an environment (i.e., water immersion) with the application of a specific load, because it would represent the compressed state of the OPS mechanism.

To minimize the effect of geometric variation in the aging analysis, it is worth using more sophisticated 3D printing techniques to produce the compliant mechanisms. An infill percentage close to 100% is also desirable to prevent a faster aging degradation process of the mechanisms. A higher number of samples is necessary to minimize a possible geometric variation impact.

Finally, increasing the aging time will allow us to understand in greater detail the aging processes over the compliant mechanisms.

Bibliography

[1] Tsai, L. W., *Mechanism design: enumeration of kinematic structures according to function*. CRC press, 2000.

[2] Howell, L. L., *Compliant Mechanisms*. A Wiley-Interscience publication, Wiley, 2001.

[3] Kumar, B. G., Singh, R. P., and Nakamura, T., "Degradation of carbon fiber-reinforced epoxy composites by ultraviolet radiation and condensation", *Journal of Composite materials*, vol. 36, no. 24, pp. 2713–2733, 2002.

[4] Ghasemi-Kahrizsangi, A., Shariatpanahi, H., Neshati, J., and Akbarinezhad, E., "Degradation of modified carbon black/epoxy nanocomposite coatings under ultraviolet exposure", *Applied Surface Science*, vol. 353, pp. 530–539, 2015.

[5] Park, J.-M., Shin, P.-S., Wang, Z.-J., Kwon, D.-J., Choi, J.-Y., Lee, S.-I., and DeVries, K. L., "The change in mechanical and interfacial properties of gf and cf reinforced epoxy composites after aging in nacl solution", *Composites Science and Technology*, vol. 122, pp. 59–66, 2016.

[6] Becerra, A. and d'Almeida, J., "Uv effects on the tensile and creep behaviour of hdpe", *Polymers and Polymer Composites*, vol. 25, no. 5, pp. 327–332, 2017.

[7] Weitsman, Y. J., *Fluid effects in polymers and polymeric composites*. Springer Science & Business Media, 2011.

[8] Capiel, G., Uicich, J., Fasce, D., and Montemartini, P. E., "Diffusion and hydrolysis effects during water aging on an epoxy-anhydride system", *Polymer degradation and stability*, vol. 153, pp. 165–171, 2018.

[9] Zhou, J. and Lucas, J. P., "Hygrothermal effects of epoxy resin. part ii: variations of glass transition temperature", *Polymer*, vol. 40, no. 20, pp. 5513–5522, 1999.

[10] Hu, Y., Li, X., Lang, A. W., Zhang, Y., and Nutt, S. R., "Water immersion aging of polydicyclopentadiene resin and glass fiber composites", *Polymer Degradation and Stability*, vol. 124, pp. 35–42, 2016.

[11] Parise, J. J., Howell, L. L., and Magleby, S. P., "Ortho-planar linear-motion springs", *Mechanism and machine theory*, vol. 36, no. 11-12, pp. 1281–1299, 2001.

[12] Howell, L. L., Magleby, S. P., and Olsen, B. M., *Handbook of compliant mechanisms*. John Wiley & Sons, 2013.

[13] Hoetmer, K., Herder, J. L., and Kim, C. J., "A building block approach for the design of statically balanced compliant mechanisms", in *ASME 2009 International Design Engineering Technical Conferences and Computers and Information in Engineering Conference*, pp. 313–323, American Society of Mechanical Engineers Digital Collection, 2009.

[14] Gou, Y., Chen, G., and Howell, L. L., "A design approach to fully compliant multistable mechanisms employing a single bistable mechanism", *Mechanics Based Design of Structures and Machines*, pp. 1–24, 2019.

[15] Zhao, L., Yu, X., Li, P., and Qiao, Y., "High-precision compliant mechanism for lens xy micro-adjustment", *Review of Scientific Instruments*, vol. 91, no. 3, p. 035004, 2020.

[16] Kozuka, H., Arata, J., Okuda, K., Onaga, A., Ohno, M., Sano, A., and Fujimoto, H., "A bio-inspired compliant parallel mechanism for high-precision robots", in *2012 IEEE International Conference on Robotics and Automation*, pp. 3122–3127, IEEE, 2012.

[17] Kennedy, J. A., Howell, L. L., and Greenwood, W., "Compliant high-precision e-quintet ratcheting (cheqr) mechanism for safety and arming devices", *Precision engineering*, vol. 31, no. 1, pp. 13–21, 2007.

[18] George B, L. and Bharanidaran, R., "Design of multifunctional compliant forceps for medical application", *Australian Journal of Mechanical Engineering*, pp. 1–5, 2020.

[19] Rubbert, L., Renaud, P., and Gangloff, J., "Design and optimization for a cardiac active stabilizer based on planar parallel compliant mechanisms", in *Engineering Systems Design and Analysis*, vol. 44861, pp. 235–244, American Society of Mechanical Engineers, 2012.

[20] Mareta, S., Halim, D., and Popov, A. A., "Control of vehicle vibration using the combined compliant actuator and suspension system", in *2015 IEEE International Conference on Mechatronics and Automation (ICMA)*, pp. 1875–1880, IEEE, 2015.

[21] Nair Prakashah, H. and Zhou, H., "Synthesis of constant torque compliant mechanisms", *Journal of Mechanisms and Robotics*, vol. 8, no. 6, 2016.

[22] Hu, R., Venkiteswaran, V., and Su, H.-J., "A variable stiffness robotic arm using linearly actuated compliant parallel guided mechanism", in *IFToMM Symposium on Mechanism Design for Robotics*, pp. 33–40, Springer, 2018.

[23] Gu, X., Li, C., Xiao, X., Lim, C. M., and Ren, H., "A compliant transoral surgical robotic system based on a parallel flexible mechanism", *Annals of biomedical engineering*, vol. 47, no. 6, pp. 1329–1344, 2019.

[24] Miao, Y. and Zheng, J., "Optimization design of compliant constant-force mechanism for apple picking actuator", *Computers and Electronics in Agriculture*, vol. 170, p. 105232, 2020.

[25] Pham, M. T., Teo, T. J., Yeo, S. H., Wang, P., and Nai, M. L. S., "A 3-d printed ti-6al-4v 3-dof compliant parallel mechanism for high precision manipulation", *IEEE/ASME Transactions on Mechatronics*, vol. 22, no. 5, pp. 2359–2368, 2017.

[26] Wang, M. and Hang, L., "Research and application of variable dof compliant five-bar mechanism based on novel compliant torsion joint in vehicle side door latch", *Proceedings of the Institution of Mechanical Engineers, Part C: Journal of Mechanical Engineering Science*, vol. 234, no. 19, pp. 3789–3808, 2020.

[27] Jeon, Y., Chu, K., Kim, J., and Seo, T., "Singularity-inducing compliant toggle linkage mechanism for large clamping range", *Mechanism and Machine Theory*, vol. 135, pp. 40–53, 2019.

[28] Chen, S., Wang, B., Zhu, S., Tan, X., Hu, J., Lian, X., Wang, L., and Wu, L., "A novel composite negative stiffness structure for recoverable trapping energy", *Composites Part A: Applied Science and Manufacturing*, vol. 129, p. 105697, 2020.

[29] Howell, L. L. and Midha, A., "A method for the design of compliant mechanisms with small-length flexural pivots", *Journal of Mechanical Design*, 1994.

[30] Hopkins, J. B. and Culpepper, M. L., "Synthesis of multi-degree of freedom, parallel flexure system concepts via freedom and constraint topology (fact)–part i: Principles", *Precision Engineering*, vol. 34, no. 2, pp. 259–270, 2010.

[31] Sigmund, O., "On the design of compliant mechanisms using topology optimization", *Journal of Structural Mechanics*, vol. 25, no. 4, pp. 493–524, 1997.

[32] Zhu, B., Chen, Q., Jin, M., and Zhang, X., "Design of fully decoupled compliant mechanisms with multiple degrees of freedom using topology optimization", *Mechanism and Machine Theory*, vol. 126, pp. 413–428, 2018.

[33] Ma, F. and Chen, G., "Chained beam-constraint-model (cbcm): a powerful tool for modeling large and complicated deflections of flexible beams in compliant mechanisms", in *International Design Engineering Technical Conferences and Computers and Information in Engineering Conference*, vol. 46360, p. V05AT08A027, American Society of Mechanical Engineers, 2014.

[34] Correa, D. M., "Design and evaluation of negative stiffness honeycombs for recoverable shock isolation", Master's thesis, The University of Texas at Austin, 2015.

[35] Howell, L. L. and Midha, A., "Parametric deflection approximations for end-loaded, large-deflection beams in compliant mechanisms", *Journal of Mechanical Design*, 1995.

[36] ASTM, "Iso/astm 52900: 2015 additive manufacturing-general principles-terminology", *ASTM F2792-10e1*, 2012.

[37] Sher, D., "The global additive manufacturing market 2018 is worth $9.3 billion - 3d printing media network." https://www.3dprintingmedia.network/the-global-additive-manufacturing-market-2018-is-worth-9-3-billion, December 2018. (Accessed on 07/04/2020).

[38] Dizon, J. R. C., Espera Jr, A. H., Chen, Q., and Advincula, R. C., "Mechanical characterization of 3d-printed polymers", *Additive Manufacturing*, vol. 20, pp. 44–67, 2018.

[39] Klatt, T. D., "Extreme energy absorption: the design, modeling, and testing of negative stiffness metamaterial inclusions", Master's thesis, The University of Texas at Austin, 2013.

[40] Alok, P., "Application of additively manufactured conformal negative stiffness honeycombs for impact isolation in protective headgear", Master's thesis, The University of Texas at Austin, 2018.

[41] Varotsis, A. B., "Introduction to fdm 3d printing | 3d hubs." https://www.3dhubs.com/knowledge-base/introduction-fdm-3d-printing. (Accessed on 07/05/2020).

[42] Cain, P., "Selecting the optimal shell and infill parameters for fdm 3d printing | 3d hubs." `https://www.3dhubs.com/knowledge-base/selecting-optimal-shell-and-infill-parameters-fdm-3d-printing/`. (Accessed on 07/05/2020).

[43] Panda, B. N., Shankhwar, K., Garg, A., and Jian, Z., "Performance evaluation of warping characteristic of fused deposition modelling process", *The International Journal of Advanced Manufacturing Technology*, vol. 88, no. 5-8, pp. 1799–1811, 2017.

[44] Wang, S., Ma, Y., Deng, Z., Zhang, S., and Cai, J., "Effects of fused deposition modeling process parameters on tensile, dynamic mechanical properties of 3d printed polylactic acid materials", *Polymer Testing*, p. 106483, 2020.

[45] Rankouhi, B., Javadpour, S., Delfanian, F., and Letcher, T., "Failure analysis and mechanical characterization of 3d printed abs with respect to layer thickness and orientation", *Journal of Failure Analysis and Prevention*, vol. 16, no. 3, pp. 467–481, 2016.

[46] Oceanz, S., "How to design parts for sls 3d printing | 3d hubs." https://www.3dhubs.com/knowledge-base/how-design-parts-sls-3d-printing. (Accessed on 07/05/2020).

[47] Dotchev, K. and Yusoff, W., "Recycling of polyamide 12 based powders in the laser sintering process", *Rapid Prototyping Journal*, 2009.

[48] Singh, R., Fraternali, F., Farina, I., and Hashmi, M. S., "Experimental investigations for development of hybrid feed stock filament of fused deposition modeling", in *Reference Module in Materials Science and Materials Engineering*, Elsevier, 2018.

[49] Feng, L., Wang, Y., and Wei, Q., "Pa12 powder recycled from sls for fdm", *Polymers*, vol. 11, no. 4, p. 727, 2019.

[50] Zarringhalam, H., Hopkinson, N., Kamperman, N., and De Vlieger, J., "Effects of processing on microstructure and properties of sls nylon 12", *Materials Science and Engineering: A*, vol. 435, pp. 172–180, 2006.

[51] Bourell, D. L., Watt, T. J., Leigh, D. K., and Fulcher, B., "Performance limitations in polymer laser sintering", *Physics Procedia*, vol. 56, pp. 147–156, 2014.

[52] Majewski, C., Zarringhalam, H., and Hopkinson, N., "Effect of the degree of particle melt on mechanical properties in selective laser-sintered nylon-12 parts", *Proceedings of the Institution of Mechanical Engineers, Part B: Journal of Engineering Manufacture*, vol. 222, no. 9, pp. 1055–1064, 2008.

[53] Ajoku, U., Saleh, N., Hopkinson, N., Hague, R., and Erasenthiran, P., "Investigating mechanical anisotropy and end-of-vector effect in laser-sintered nylon parts", *Proceedings of the Institution of Mechanical Engineers, Part B: Journal of Engineering Manufacture*, vol. 220, no. 7, pp. 1077–1086, 2006.

[54] Kim, G. and Oh, Y., "A benchmark study on rapid prototyping processes and machines: quantitative comparisons of mechanical properties, accuracy, roughness, speed, and material cost", *Proceedings of the Institution of Mechanical Engineers, Part B: Journal of Engineering Manufacture*, vol. 222, no. 2, pp. 201–215, 2008.

[55] Armstrong, C., "Post processing for fdm printed parts | 3d hubs." https://www.3dhubs.com/knowledge-base/post-processing-fdm-printed-parts. (Accessed on 07/07/2020).

[56] Redwood, B., "Post processing for sls printed parts | 3d hubs." https://www.3dhubs.com/knowledge-base/post-processing-sls-printed-parts. (Accessed on 07/07/2020).

[57] Zhang, M., Song, X., Grove, W., Hull, E., Pei, Z., Ning, F., and Cong, W., "Carbon nanotube reinforced fused deposition modeling using microwave irradiation", in *ASME 2016 11th International Manufacturing Science and Engineering Conference*, American Society of Mechanical Engineers Digital Collection, 2016.

[58] Shaw, B. and Dirven, S., "Investigation of porosity and mechanical properties of nylon sls structures", in *2016 23rd International Conference on Mechatronics and Machine Vision in Practice (M2VIP)*, pp. 1–6, IEEE, 2016.

[59] Chanda, M., *Plastics technology handbook*. CRC press, 2017.

[60] Fink, J. K., *Handbook of engineering and specialty thermoplastics, Volume 1: Polyolefins and Styrenics*, vol. 1. John Wiley & Sons, 2010.

[61] Wang, J., GangaRao, H., Liang, R., Zhou, D., Liu, W., and Fang, Y., "Durability of glass fiber-reinforced polymer composites under the combined effects of moisture and sustained loads", *Journal of Reinforced Plastics and Composites*, vol. 34, no. 21, pp. 1739–1754, 2015.

[62] Lu, T., Solis-Ramos, E., Yi, Y., and Kumosa, M., "Particle removal mechanisms in synergistic aging of polymers and glass reinforced polymer composites under combined uv and water", *Composites Science and Technology*, vol. 153, pp. 273–281, 2017.

[63] Lu, T., Solis-Ramos, E., Yi, Y.-B., and Kumosa, M., "Synergistic environmental degradation of glass reinforced polymer composites", *Polymer Degradation and Stability*, vol. 131, pp. 1–8, 2016.

[64] Lu, T., Solis-Ramos, E., Yi, Y., and Kumosa, M., "Uv degradation model for polymers and polymer matrix composites", *Polymer degradation and stability*, vol. 154, pp. 203–210, 2018.

[65] Santos, L. F. L.dos, "O efeito da umidade, temperatura e ultravioleta no comportamento mecânico de estruturas sanduíche com miolo de espuma e honeycomb de papelão", tech. rep., Universidade do Estado do Rio de Janeiro, Rio de Janeiro, RJ, July 2019.

[66] Vichi, A., Ferrari, M., and Davidson, C. L., "Color and opacity variations in three different resin-based composite products after water aging", *Dental Materials*, vol. 20, no. 6, pp. 530–534, 2004.

[67] Martínez-Romo, A., Mota, R. G., Bernal, J. S., Reyes, C. F., and Candelas, I. R., "Effect of ultraviolet radiation in the photo-oxidation of high density polyethylene and biodegradable polyethylene films", in *Journal of Physics: Conference Series*, vol. 582, p. 012026, IOP Publishing, 2015.

[68] ASTM, "Standard terminology relating to plastics", 2012.

[69] Zafar, A., Bertocco, F., Schjødt-Thomsen, J., and Rauhe, J., "Investigation of the long term effects of moisture on carbon fibre and epoxy matrix composites", *Composites Science and Technology*, vol. 72, no. 6, pp. 656–666, 2012.

[70] d'Almeida, J. R. and Ottolini, L. M., "Analysis of the compression behavior of an e-glass composite pipe after aging in water", *Polymers and Polymer Composites*, p. 0967391119895735, 2019.

[71] Yu, Y.-J., Hearon, K., Wilson, T. S., and Maitland, D. J., "The effect of moisture absorption on the physical properties of polyurethane shape memory polymer foams", *Smart Materials and Structures*, vol. 20, no. 8, p. 085010, 2011.

[72] Kajorncheappunngam, S., Gupta, R. K., and GangaRao, H. V., "Effect of aging environment on degradation of glass-reinforced epoxy", *Journal of composites for construction*, vol. 6, no. 1, pp. 61–69, 2002.

[73] Colin, X. and Verdu, J., "Humid ageing of organic matrix composites", in *Durability of composites in a marine environment*, pp. 47–114, Springer, 2014.

[74] Amaral, D. L., "Envelhecimento de polímeros empregados na indústria de Óleo e gás", tech. rep., Universidade do Estado do Rio de Janeiro, Rio de Janeiro, RJ, Aug. 2020.

[75] Pereira, A. A. C., d'Almeida, J. R. M., and Castro, T. M. L., "Evaluation of short-term creep behavior of pe-hd after aging in oil derivatives", *Polymers and Polymer Composites*, vol. 26, no. 3, pp. 243–250, 2018.

[76] Hernández, J. L. M. and d'Almeida, J. R. M., "Aging of polyamide 12 in oil at different temperatures and pressures", *Polymers for Advanced Technologies*, vol. 28, no. 12, pp. 1778–1786, 2017.

[77] Heshmati, M., Haghani, R., and Al-Emrani, M., "Effects of moisture on the long-term performance of adhesively bonded frp/steel joints used in bridges", *Composites Part B: Engineering*, vol. 92, pp. 447–462, 2016.

[78] Pomiès, F., Carlsson, L., and Gillespie, J., "Marine environmental effects on polymer matrix composites", in *Composite Materials: Fatigue and Fracture: Fifth Volume*, ASTM International, 1995.

[79] Callister, W. D. *et al.*, *Fundamentals of materials science and engineering*, vol. 471660817. Wiley London, 2000.

[80] Plessix, B.de Parscau du, Jacquemin, F., Lefébure, P., and Le Corre, S., "Characterization and modeling of the polymerization-dependent moisture absorption behavior of an epoxy-carbon fiber-reinforced composite material", *Journal of Composite Materials*, vol. 50, no. 18, pp. 2495–2505, 2016.

[81] Robert, M., Wang, P., Cousin, P., and Benmokrane, B., "Temperature as an accelerating factor for long-term durability testing of frps: Should there be any limitations?", *Journal of Composites for Construction*, vol. 14, no. 4, pp. 361–367, 2010.

[82] Bociąga, E. and Trzaskalska, M., "Influence of ageing on the gloss, color, and structure of colored abs", *Color Research & Application*, vol. 41, no. 4, pp. 392–398, 2016.

[83] Boldizar, A. and Möller, K., "Degradation of abs during repeated processing and accelerated ageing", *Polymer degradation and stability*, vol. 81, no. 2, pp. 359–366, 2003.

[84] Fiorio, R., Villanueva Díez, S., Sánchez, A., D'hooge, D. R., and Cardon, L., "Influence of different stabilization systems and multiple ultraviolet a (uva) aging/recycling steps on physicochemical, mechanical, colorimetric, and thermal-oxidative properties of abs", *Materials*, vol. 13, no. 1, p. 212, 2020.

[85] Li, J., Chen, F., Yang, L., Jiang, L., and Dan, Y., "Ftir analysis on aging characteristics of abs/pc blend under uv-irradiation in air", *Spectrochimica Acta Part A: Molecular and Biomolecular Spectroscopy*, vol. 184, pp. 361–367, 2017.

[86] Kakanuru, P. and Pochiraju, K., "Moisture ingress and degradation of additively manufactured pla, abs and pla/sic composite parts", *Additive Manufacturing*, vol. 36, p. 101529, 2020.

[87] Popescu, D., Baciu, F., Vlăsceanu, D., Cotruţ, C. M., and Marinescu, R., "Effects of multiple sterilizations and natural aging on the mechanical behavior of 3d-printed abs", *Mechanics of Materials*, vol. 148, p. 103423, 2020.

[88] Goodridge, R., Hague, R., and Tuck, C., "Effect of long-term ageing on the tensile properties of a polyamide 12 laser sintering material", *Polymer Testing*, vol. 29, no. 4, pp. 483–493, 2010.

[89] ASTM, "Standard test method for tensile properties of plastics", 2014.

[90] Puri, G., *Python Scripts for ABAQUS: learn by example*. Gautam Puri, 2011.

[91] Hibbeler, R. C., *Mechanics of Materials*. Pearson, 2007.

[92] Howell, L. L., Midha, A., and Norton, T. W., "Evaluation of equivalent spring stiffness for use in a pseudo-rigid-body model of large-deflection compliant mechanisms", *Journal of Mechanical Design*, 1996.

[93] Desloir, M., Benoit, C., Bendaoud, A., Alcouffe, P., and Carrot, C., "Plasticization of poly (vinyl butyral) by water: Glass transition temperature and mechanical properties", *Journal of Applied Polymer Science*, vol. 136, no. 12, p. 47230, 2019.

[94] Pereira, A. A. C., Becerra, A. F. C., and Moraes, J. R., "Análise dos efeitos de envelhecimento em óleo sobre a coloração e as propriedades mecânicas do pead", 2018.

A
Dimensions of the ortho-planar spring specimens

In this appendix, the experimental data containing the dimensions of each ortho-planar spring specimen is shown. In Table A.1, the values of diameter, thickness and weight before and after aging are listed. In Table A.2, the values of the width of each member of the legs of the specimens is listed and in Table B.2 the infill percentage of each OPS sample is presented.

Table A.1: Diameter, thickness and weight before and after aging of the ortho-planar spring specimens.

No.	Condition	Diameter (mm)	Thickness (mm)	Weight (g)	Weight after (g)
1	AR	119.97	3.1	23.76	-
2	AR	119.66	3.36	24.96	-
3	AR	119.36	3.27	25.02	-
4	UV	119.13	3.17	24.50	24.61
5	UV	119.93	3.08	23.86	23.98
6	UV	119.62	3.27	24.53	24.65
7	WI-RT	119.56	3.48	24.96	25.79
8	WI-RT	119.06	3.07	24.66	25.28
9	WI-RT	119.36	3.46	24.73	25.73
10	WI-50	120.25	3.34	22.75	23.84
11	WI-50	119.7	2.93	22.52	23.95
12	WI-50	119.18	3.33	24.86	25.73
13	WI-70	119.3	3.31	25.12	26.19
14	WI-70	119.16	3.14	25.63	26.41
15	WI-70	118.83	3.52	25.83	27.62
16	OI-RT	119.4	3.29	24.97	25.76
17	OI-RT	118.6	3.13	23.03	23.91
18	OI-RT	119.05	3.45	25.29	26.15
19	OI-50	119.26	3.59	25.58	26.46
20	OI-50	119.15	3.32	25.16	26.46
21	OI-50	118.55	3.41	25.23	26.33
22	OI-70	119.26	3.54	25.66	26.50
23	OI-70	118.68	3.24	22.86	23.88
24	OI-70	119.35	3.59	24.68	26.18

Table A.2: Width of each flexible member of the legs of the ortho-planar spring specimens.

No.	Condition	Member 1 (mm)	Member 2 (mm)	Member 3 (mm)	Member 4 (mm)	Member 5 (mm)	Member 6 (mm)
1	AR	3.53	3.55	3.62	3.64	3.62	3.64
2	AR	3.42	3.53	3.56	3.58	3.53	3.53
3	AR	3.75	3.64	3.82	3.86	3.83	3.86
4	UV	3.59	3.48	3.55	3.56	3.55	3.6
5	UV	3.57	3.54	3.56	3.5	3.59	3.54
6	UV	3.95	3.91	3.74	3.91	4.22	3.89
7	WI-RT	3.6	3.54	3.59	3.53	3.47	3.57
8	WI-RT	3.49	3.44	3.63	3.79	3.58	3.64
9	WI-RT	3.42	3.3	3.36	3.37	3.32	3.35
10	WI-50	3.51	3.58	3.4	3.49	3.49	3.48
11	WI-50	3.65	3.48	3.67	3.84	3.46	3.56
12	WI-50	3.63	3.61	3.71	3.67	3.72	3.58
13	WI-70	3.97	3.83	3.54	3.75	3.79	3.87
14	WI-70	3.87	3.91	3.8	3.75	3.73	3.71
15	WI-70	3.97	3.54	3.87	3.86	3.55	3.9
16	OI-RT	3.77	3.71	3.74	3.66	3.68	3.73
17	OI-RT	3.48	3.44	3.35	3.38	3.41	3.48
18	OI-RT	3.73	3.61	3.68	3.61	3.44	3.69
19	OI-50	3.91	4.03	3.85	3.77	3.96	3.83
20	OI-50	3.51	3.71	3.62	3.68	3.58	3.53
21	OI-50	3.41	3.47	3.46	3.44	3.47	3.47
22	OI-70	3.63	3.61	3.55	3.63	3.69	3.81
23	OI-70	3.36	3.37	3.48	3.45	3.54	3.55
24	OI-70	3.28	3.43	3.36	3.31	3.41	3.23

Table A.3: Calculated infill percentage of the OPS samples.

No.	Condition	Infill (%)
1	AR	93.99
2	AR	91.12
3	AR	93.85
4	UV	94.80
5	UV	94.99
6	UV	92.00
7	WI-RT	87.98
8	WI-RT	98.52
9	WI-RT	87.65
10	WI-50	83.55
11	WI-50	94.26
12	WI-50	91.56
13	WI-70	93.07
14	WI-70	99.13
15	WI-70	90.00
16	OI-RT	93.09
17	OI-RT	90.23
18	OI-RT	89.89
19	OI-50	87.38
20	OI-50	92.94
21	OI-50	90.72
22	OI-70	88.90
23	OI-70	86.54
24	OI-70	84.31

B
Dimensions of the tensile test specimens

In this appendix, the experimental data containing the dimensions of each tensile test specimen is shown. In Table B.1, the values of length, widths, thickness and weight before and after aging are listed and in Table A.3 the infill percentage of each tensile sample is presented.

Table B.1: Length, widths, thickness and weight before and after aging of the tensile test samples.

No.	Condition	Length (mm)	Width left (mm)	Width right (mm)	Width center (mm)	Thickness (mm)	Weight (g)	Weight after (g)
1	AR	163.5	18.9	18.88	12.9	3.18	6.37	-
2	AR	163.5	18.95	18.8	12.86	3.3	7.03	-
3	AR	164	18.86	18.95	12.86	3.33	5.89	-
4	UV	163.5	18.87	18.96	12.94	3.17	6.13	7.16
5	UV	163.5	18.86	18.74	12.86	3.21	6.82	7.86
6	UV	163.5	18.71	18.87	12.77	3.36	7.12	8.16
7	WI-RT	163.5	18.98	18.8	12.98	3.35	6.30	7.06
8	WI-RT	164	18.88	18.94	12.97	3.18	7.26	7.72
9	WI-RT	163.5	18.87	18.85	12.87	3.25	6.28	6.89
10	WI-50	164.5	18.91	18.86	12.93	3.24	5.60	6.60
11	WI-50	163.5	18.79	18.83	12.88	3.28	6.84	7.79
12	WI-50	164	18.91	18.81	12.88	3.25	6.61	7.98
13	WI-70	164	18.78	18.85	12.95	3.23	5.27	6.68
14	WI-70	163.5	18.73	18.79	12.87	3.29	6.69	7.95
15	WI-70	163.5	18.7	18.79	12.85	3.33	7.07	7.62
16	OI-RT	164	18.75	18.76	12.86	3.41	7.22	8.09
17	OI-RT	163.5	18.73	18.87	12.87	3.14	6.07	7.40
18	OI-RT	164	18.82	18.74	12.84	3.19	5.87	7.40
19	OI-50	163	18.76	18.89	12.94	3.37	6.46	7.88
20	OI-50	163.5	18.69	18.82	12.72	3.44	7.20	8.03
21	OI-50	163	18.75	18.73	12.87	3.26	5.96	7.35
22	OI-70	163.5	18.67	18.7	12.85	3.2	6.76	7.90
23	OI-70	163.5	18.77	18.7	12.86	3.34	6.98	8.18
24	OI-70	163	18.68	18.82	12.83	3.34	6.75	8.10

Table B.2: Calculated infill percentage of the tensile samples.

No.	Condition	Infill (%)
1	AR	74.86
2	AR	79.67
3	AR	65.82
4	UV	72.10
5	UV	79.72
6	UV	79.56
7	WI-RT	70.27
8	WI-RT	84.97
9	WI-RT	72.26
10	WI-50	60.98
11	WI-50	76.43
12	WI-50	79.96
13	WI-70	64.14
14	WI-70	78.17
15	WI-70	75.82
16	OI-RT	79.35
17	OI-RT	72.54
18	OI-RT	68.87
19	OI-50	72.06
20	OI-50	78.77
21	OI-50	69.00
22	OI-70	79.78
23	OI-70	78.73
24	OI-70	76.28

C
Plots of the mechanical tests of the tensile samples

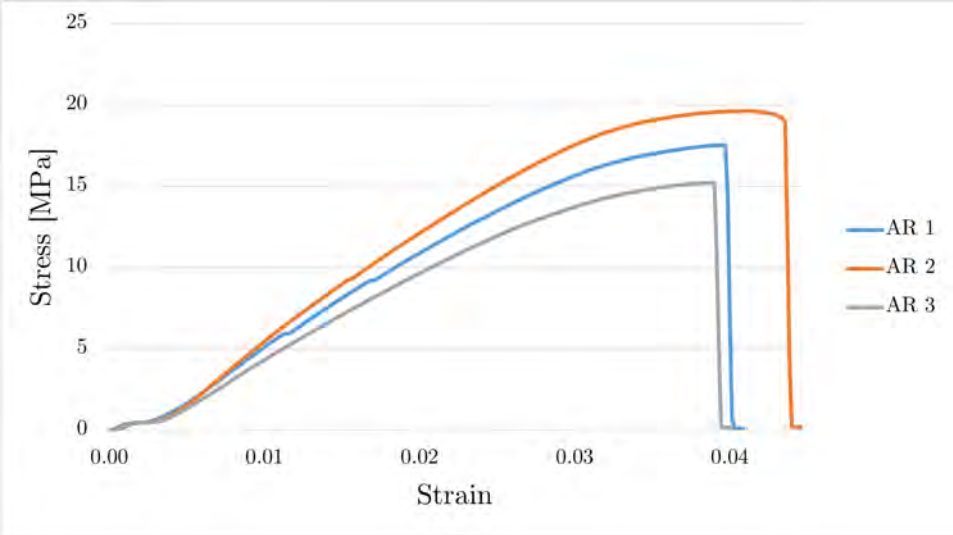

Figure C.1: Stress-strain curves of the tensile tests of the three tensile AR samples.

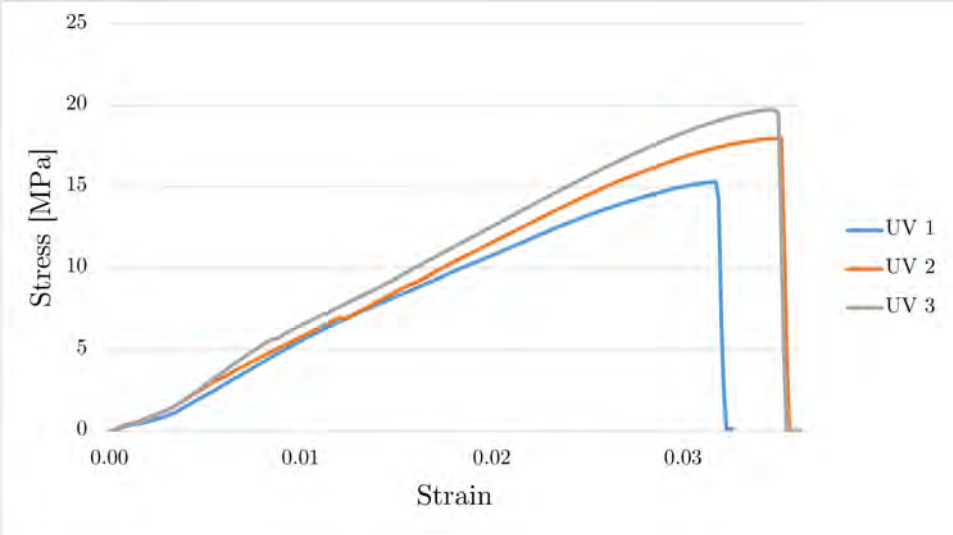

Figure C.2: Stress-strain curves of the tensile tests of the three tensile UV samples.

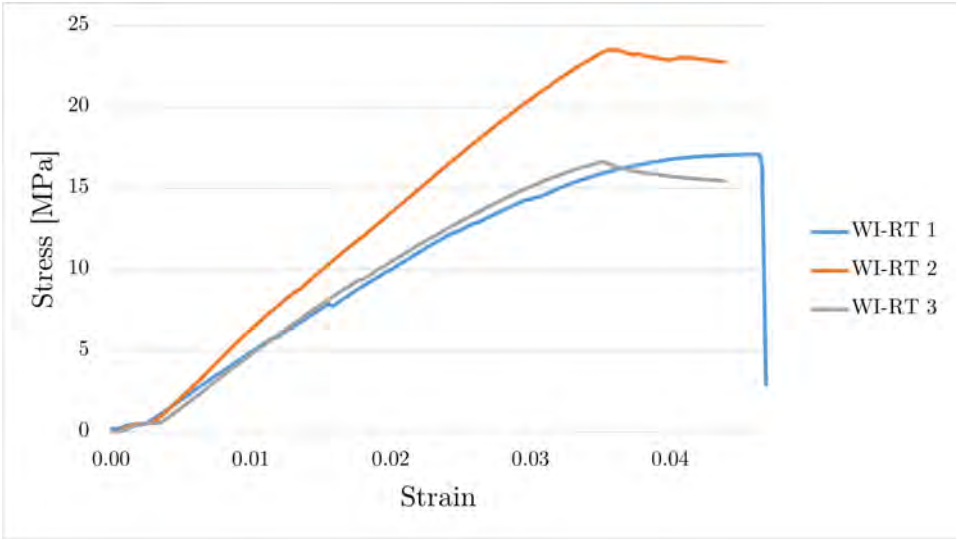

Figure C.3: Stress-strain curves of the tensile tests of the three tensile WI-RT samples.

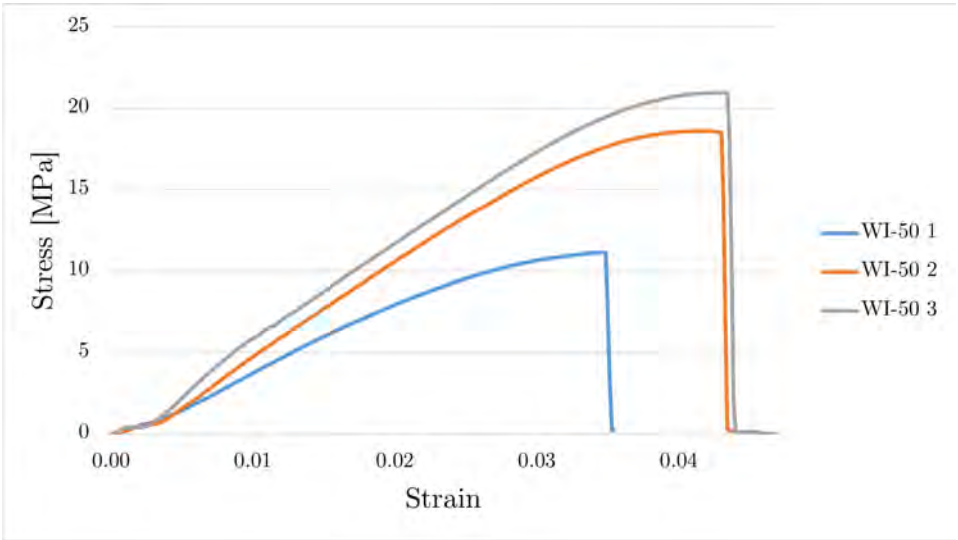

Figure C.4: Stress-strain curves of the tensile tests of the three tensile WI-50 samples.

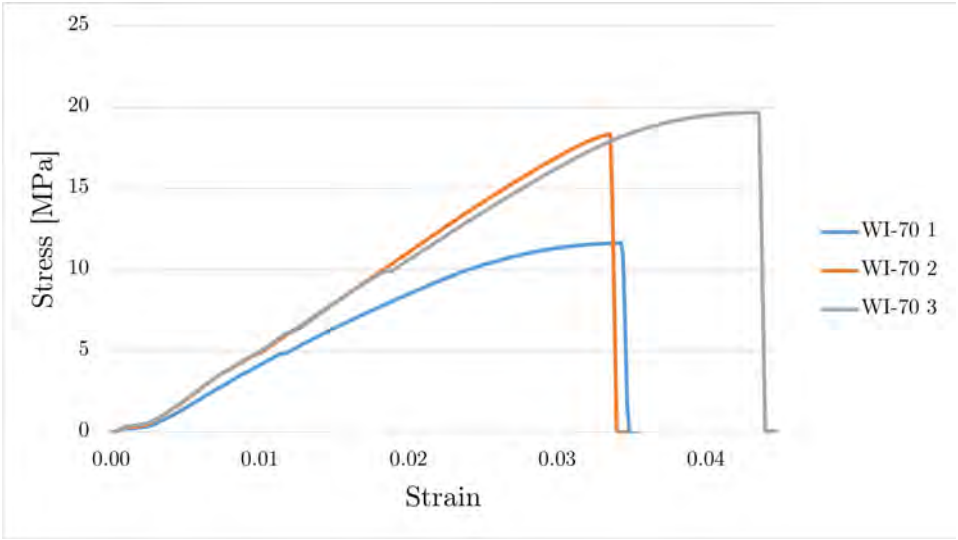

Figure C.5: Stress-strain curves of the tensile tests of the three tensile WI-70 samples.

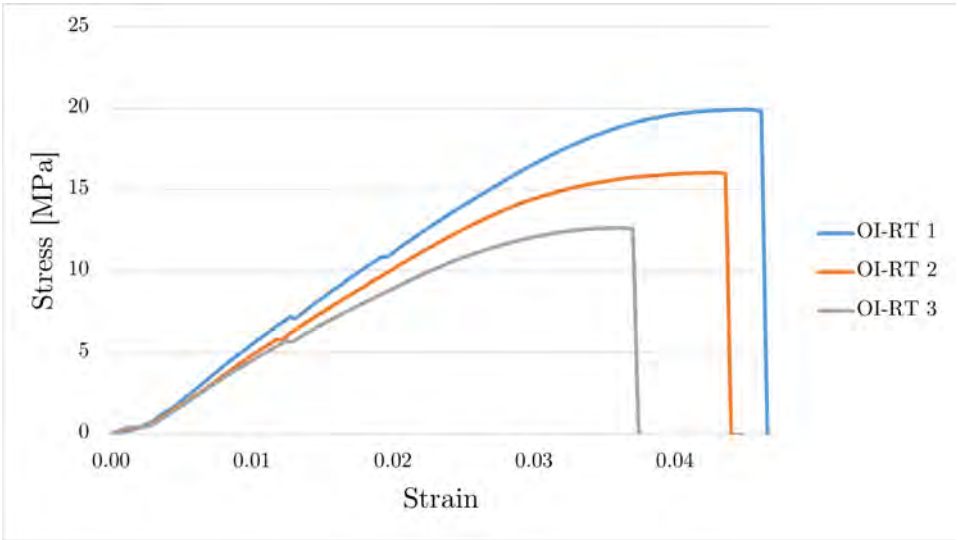

Figure C.6: Stress-strain curves of the tensile tests of the three tensile OI-RT samples.

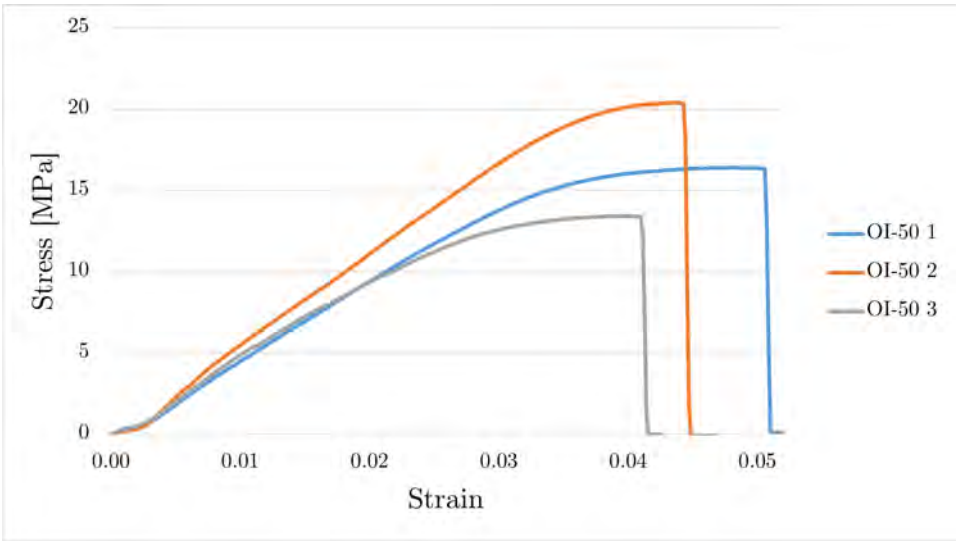

Figure C.7: Stress-strain curves of the tensile tests of the three tensile OI-50 samples.

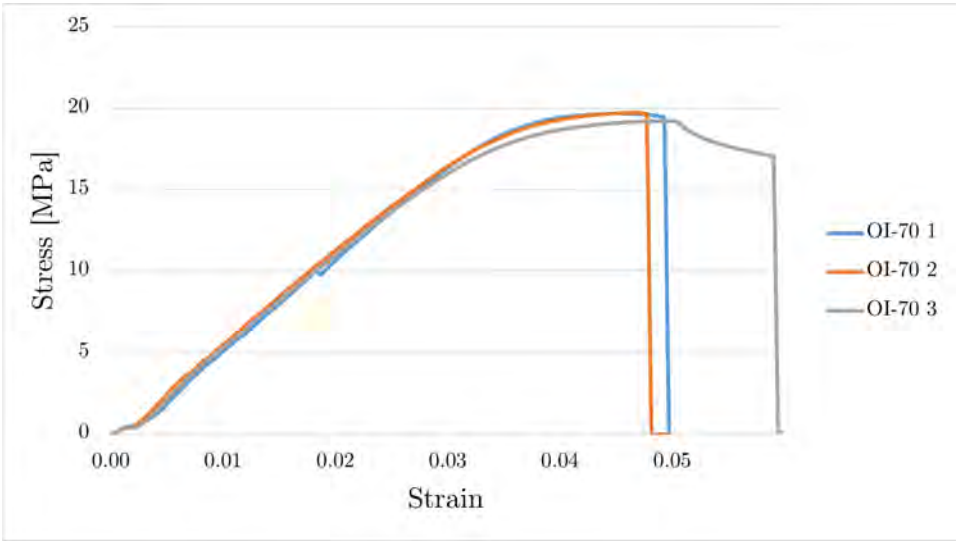

Figure C.8: Stress-strain curves of the tensile tests of the three tensile OI-70 samples.

D
Plots of the mechanical tests of the OPS samples

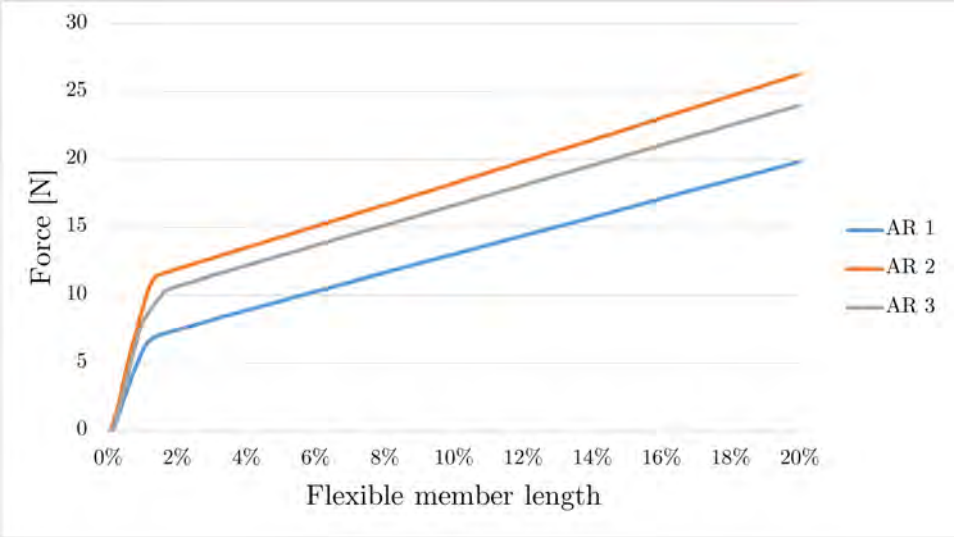

Figure D.1: Force-displacement curves of the mechanical tests of the three OPS AR samples.

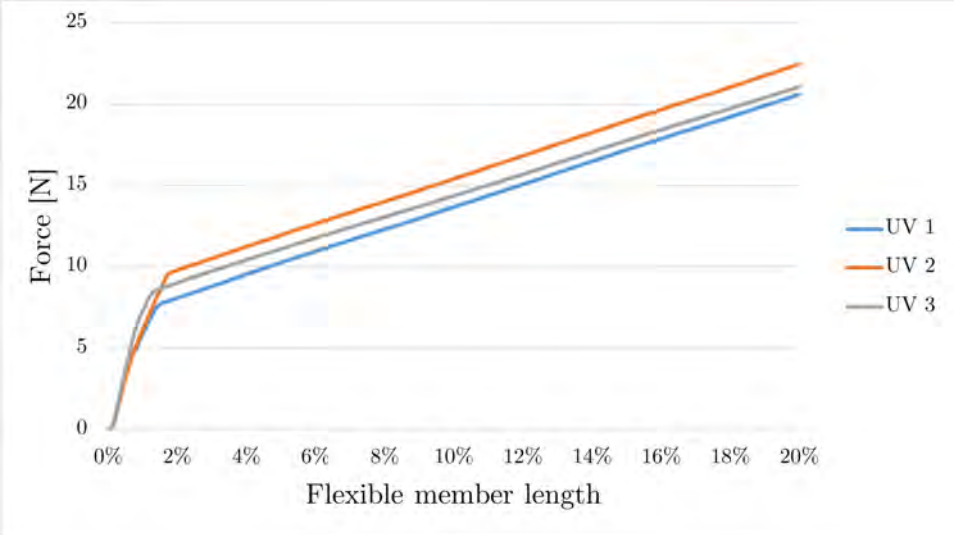

Figure D.2: Force-displacement curves of the mechanical tests of the three OPS UV samples.

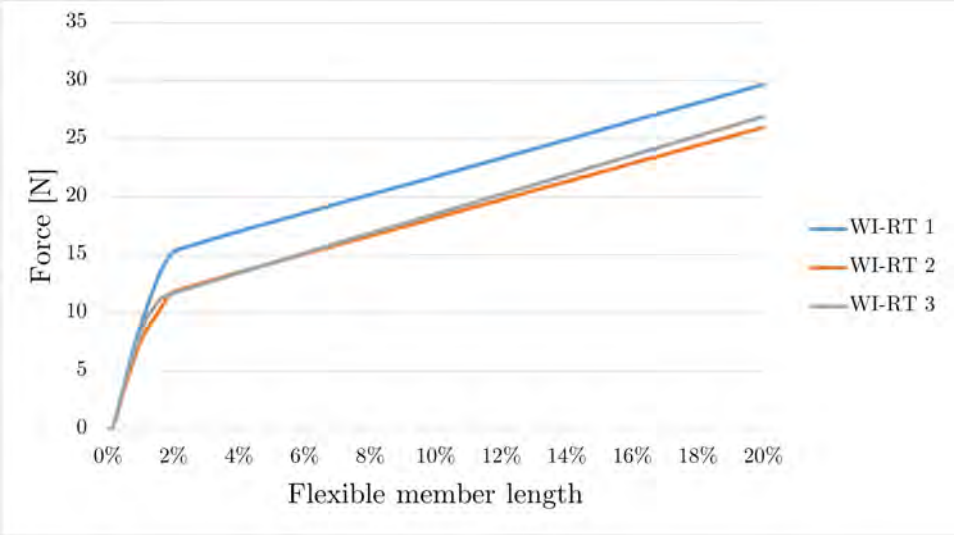

Figure D.3: Force-displacement curves of the mechanical tests of the three OPS WI-RT samples.

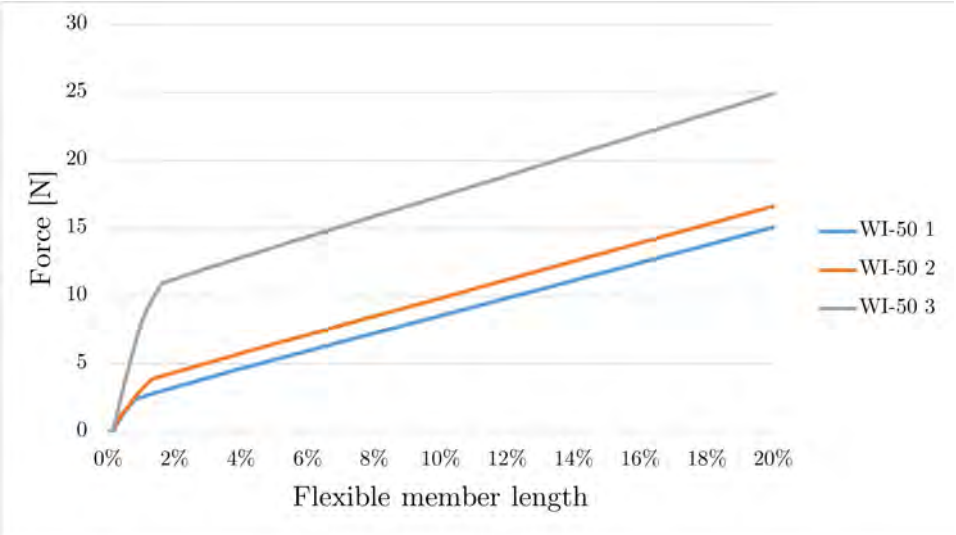

Figure D.4: Force-displacement curves of the mechanical tests of the three OPS WI-50 samples.

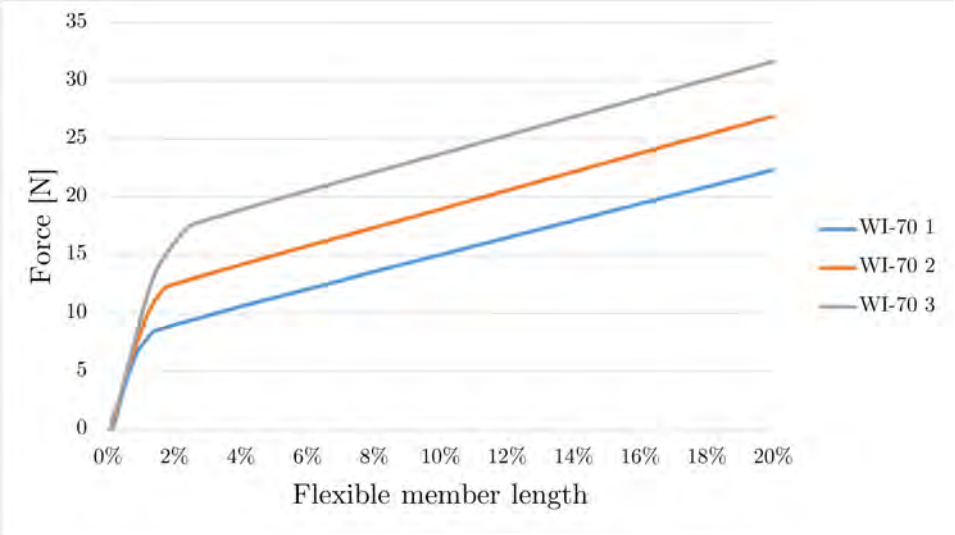

Figure D.5: Force-displacement curves of the mechanical tests of the three OPS WI-70 samples.

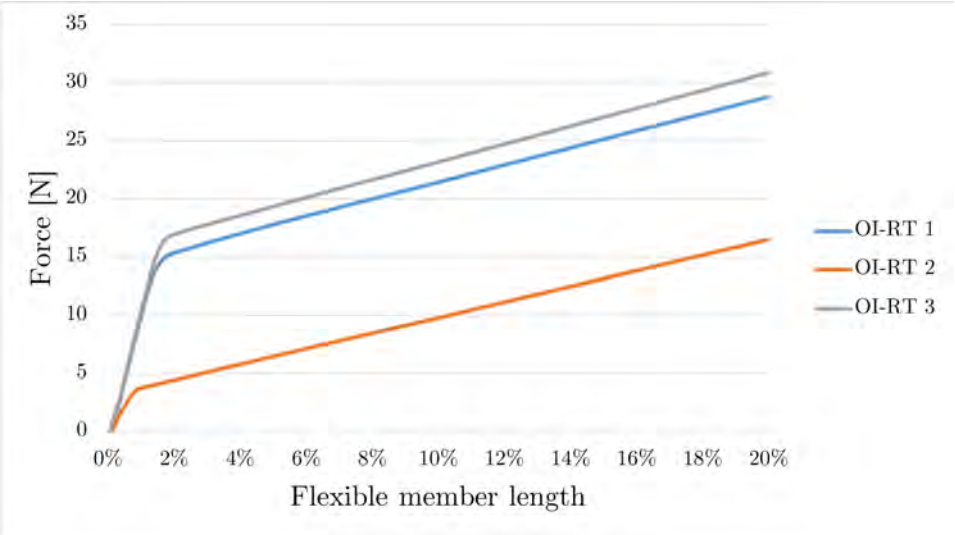

Figure D.6: Force-displacement curves of the mechanical tests of the three OPS OI-RT samples.

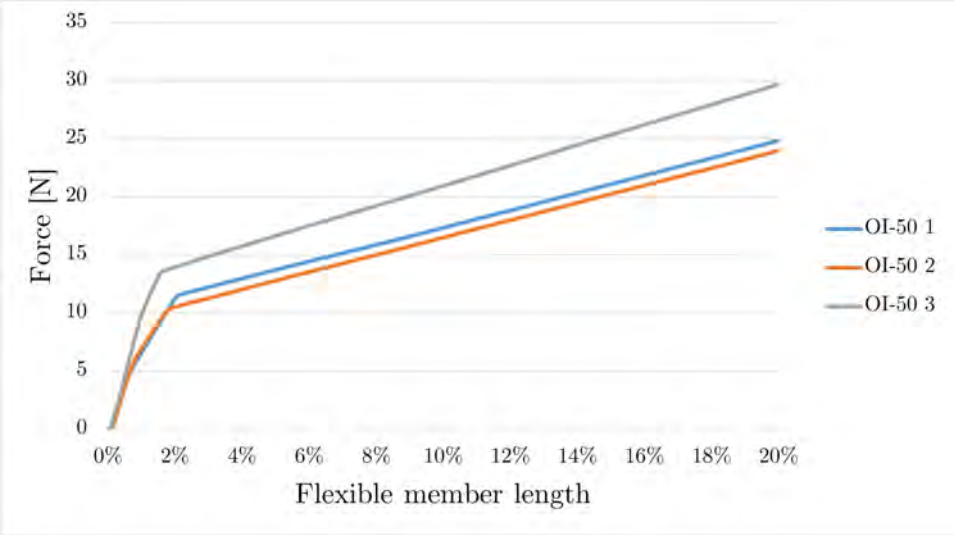

Figure D.7: Force-displacement curves of the mechanical tests of the three OPS OI-50 samples.

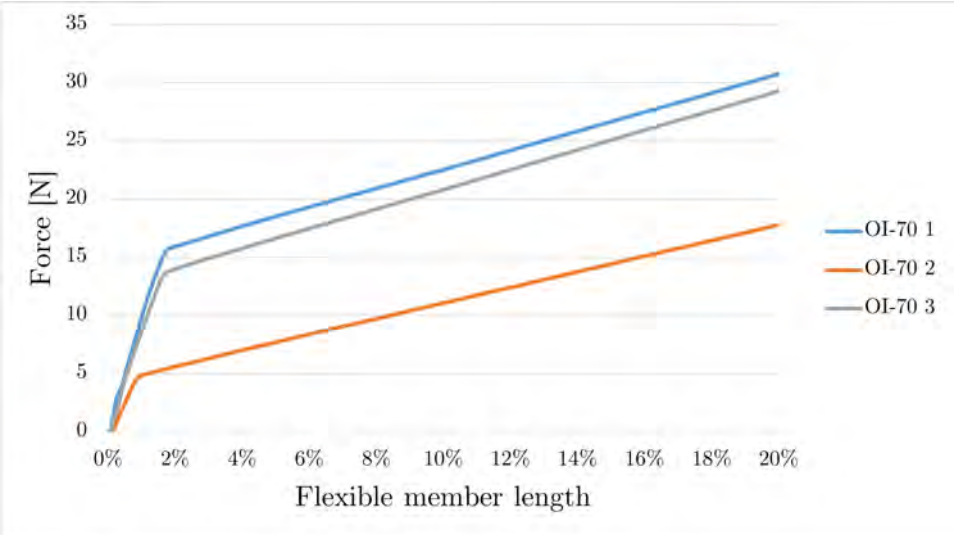

Figure D.8: Force-displacement curves of the mechanical tests of the three OPS OI-70 samples.